The Astrophysical Journal, 634:1319–1335, 2005 December 1


# SYNTHETIC LICK INDICES AND DETECTION OF $\alpha$-ENHANCED STARS. III. F, G, AND K STARS WITH [Fe/H] > 0.00

M. Franchini, C. Morossi, and P. Di Marcantonio
INAF-Osservatorio Astronomico di Trieste, Via G. B. Tiepolo, 11, I-34131 Trieste, Italy;
franchini@ts.astro.it, morossi@ts.astro.it, dimarcan@ts.astro.it

F. Castelli
Istituto di Astrofisica Spaziale e Fisica Cosmica, INAF-Osservatorio Astronomico di Trieste,
Via G. B. Tiepolo, 11, I-34131 Trieste, Italy; castelli@ts.astro.it

M. L. Malagnini
Dipartimento di Astronomia, Università degli Studi di Trieste, Via G. B. Tiepolo, 11, I-34131 Trieste, Italy; malagnini@ts.astro.it

and

M. Chavez
Instituto Nacional de Astrofísica, Optica, y Electrónica, Apartados postales 51 y 216, 72000 Puebla, Mexico; mchavez@inaoep.mx
*Received 2005 May 23; accepted 2005 July 29*

## ABSTRACT

A sample of 119 F, G, and K solar neighborhood stars, selected under the condition $[\mathrm{Fe/H}] > 0.00$, is investigated in order to detect which of them, if any, present $\alpha$-enhanced characteristics. According to the kinematics, the sample represents stars of the thin-disk component of the Galaxy. The search of $\alpha$-enhanced characteristics is performed by adopting an already tested procedure that does not require previous knowledge of the stellar main atmospheric parameters. The analysis is based on the comparison of spectral indices in the Lick IDS system, coming from different observational data sets, with synthetic ones computed with solar-scaled abundances and with $\alpha$-element enhancement. The main result of the analysis is the extreme paucity (likely just one in 119) of $\alpha$-enhanced stars in our sample, thus suggesting $[\alpha/\mathrm{Fe}] = 0.0$ for thin-disk stars with $[\mathrm{Fe/H}] > 0.00$. This result, which is in agreement with the standard evolutionary picture of the disk of the Galaxy, is compared with recent results from high-resolution analysis reported in the literature. The role of the atmospheric parameter assumptions in the analysis of high-resolution spectroscopic data is discussed, and a possible explanation of discrepant results about $\alpha$-enhancement for stars with $[\mathrm{Fe/H}] > 0.00$ is presented.

*Subject headings:* Galaxy: stellar content — stars: abundances — stars: kinematics — stars: late-type

*Online material:* machine-readable tables

## 1. INTRODUCTION

Theories dealing with the formation and evolution of galaxies proceed from different basic methodologies: either from dynamical *N*-body simulations or from the building up of preconstituted elementary structures. Possible scenarios include hierarchical merging and collapse phenomena and almost continuous formation of different structures. When checking predictions with observations, the more details are available, the more complex the results of the comparison of chemical and dynamical properties of stellar systems and individual stars as their tracers. Kinematics conveyed the first idea of different stellar populations in the Galaxy. "I believe that . . . there are two distinct classes of stars . . . " is probably the very beginning of the concept of stellar populations, introduced by Oort (1926), when discussing the observed asymmetry in the distribution of stellar velocities. Starting from the Baade (1958) definition of stellar Populations I and II at the historical Vatican meeting, based on chemical and dynamical properties, the complexity and richness of observations made it unavoidable to extend the number of different stellar populations and to characterize them on the basis of measured abundances and kinematical properties. The observed complexity asks for galaxy formation and evolution models in order to characterize the different substructures and depict their individual chemical and dynamical histories. The ESA *Gaia* mission is foreseen to gather accurate data about the dynamics and chemistry for an unprecedented huge number of stars; thus, substructures are expected to be more easily identified in the future (Nissen 2005).

Stellar population synthesis gained great popularity after the extraordinary work by B. Tinsley and was applied not only to spectrophotometric data, but also to selected spectral features intended for more detailed comparison with observations. The basic concept is that a galaxy is composed of several superposed stellar populations with distinct characteristics. It is therefore of fundamental importance to understand the properties of individual stars and of resolved populations if we wish to properly interpret the observed integrated features of distant systems. Nowadays, the spectral signatures are picked up with high-resolution observations of large samples of different stellar types, thus making the scenario at the same time more precise and more complex.

Galaxy models, considering the stellar components only, are helped from observations in many different electromagnetic regions of external galaxies, and the more diffuse representation almost universally accepted is actually through the stellar substructures of halo, thick and thin disks, and bulge. Each substructure is characterized by different geometric, kinematical, and chemical properties as inferred from observations; however, there are still difficulties in interpreting these substructures in terms of ages and formation histories.

Freeman & Bland-Hawthorn (2002) present and discuss the basic signatures extracted from observations that can give insight into the Galaxy formation process in the context of hierarchical

aggregation starting from a large-scale distribution of cold dark matter.

In recent years, observations of individual stars have gained a newer interest and have grown in both quantity and quality. Among others, we recall on one side high-resolution spectroscopic observations by Bensby et al. (2005), Fuhrmann (2004), Allende Prieto et al. (2004, hereafter AP04), and Spite et al. (2005), and on the other side the photometric Geneva-Copenhagen Survey of the Solar Neighbourhood (Nordström et al. 2004). Of particular relevance are the abundance and kinematical analysis of stars characterized by the so-called $\alpha$-enhancement phenomenon, which gives insights into the role, for instance, of Type I and Type II supernovae in the chemical enrichment of individual stellar populations (Chen et al. 2003). Most of the analyses refer to main-sequence or slightly evolved stars of spectral types F, G, and K because their atmospheres still preserve the original chemical composition of their birth places. The trend of the $[\alpha/\mathrm{Fe}]$ abundance ratio with $[\mathrm{Fe/H}]$ is the subject of many papers (see, e.g., Bensby et al. 2003; Reddy et al. 2003; Nissen 2005). While there are clear indications of different behaviors in the thick disk and in the $\alpha$-enhanced thin disk of the Galaxy, most of the studies show a decrease of $[\alpha/\mathrm{Fe}]$ from +0.4 at $[\mathrm{Fe/H}] < -1.0$ to $[\alpha/\mathrm{Fe}] \sim 0.0$ at $[\mathrm{Fe/H}] = 0.0$ (see also Mishenina et al. 2004) in agreement with predictions by current nucleosynthesis theories and Galactic chemical evolution models (see, e.g., Matteucci 2004). In AP04 the authors confirm that abundance ratios of $\alpha$-elements to iron become smaller as the iron abundance increases until approaching the solar values but found that "the trends reverse for higher iron abundances," thus opening a new scenario. Franchini et al. (2005, hereafter FR05) reanalyzed the stars studied by AP04 with a technique that discriminates $\alpha$-enhanced (non–solar-scaled abundance [NSSA]) stars from those with solar-scaled abundance (SSA) without requiring any assumption for the main stellar atmospheric parameters. The main results are as follows:

1. a clear consistency between FR05 classification and the $[\alpha/\mathrm{Fe}]$ abundance ratios derived by AP04 as far as the metal-poor and solar stars are concerned;
2. no detection of $\alpha$-enhanced stars with $[\mathrm{Fe/H}] > 0.0$, while there are several stars that fall more than 1 $\sigma$ above the $[\alpha/\mathrm{Fe}] = 0.0$ line in Figure 14 of AP04.

The FR05 paper suggests that the discrepancy with AP04 results may be due to the effective temperature scale adopted by AP04. In fact, by taking advantage of the dependence of the AP04 abundance ratios on the $T_{\mathrm{eff}}$ values, FR05 recomputed the $[\mathrm{Fe/H}]$ and the $[\alpha/\mathrm{Fe}]$ values of a subsample of AP04 stars by assuming a systematic offset of 125 K in the AP04 $T_{\mathrm{eff}}$ values. In this case the agreement with FR05 classification, which is independent of the assumed $T_{\mathrm{eff}}$ values, is significantly improved. On the basis of this analysis, FR05 concluded that the $[\alpha/\mathrm{Fe}]$ abundance ratio derived from the analysis of high-resolution spectra by AP04 is quite model-dependent and that the increase of $[\alpha/\mathrm{Fe}]$ at $[\mathrm{Fe/H}] > 0.0$ requires further checks.

In this paper we search a list of $[\mathrm{Fe/H}] > 0.0$ stars for $\alpha$-enhanced candidates with the aim of providing a list of targets for a follow-up analysis at high resolution to really assess the presence, in the solar neighborhood, of a population of $\alpha$-enhanced stars in the supersolar $[\mathrm{Fe/H}]$ regime.

In § 2 we present the stellar sample and the observational data sets. Section 3 contains the results of our procedure for detecting $\alpha$-enhanced stars. In § 4 we discuss our results as compared with those from recent papers dealing with the determination of individual element abundances in stars of the solar neighborhood. Concluding remarks are given in § 5.

## 2. THE STELLAR SAMPLE

As in previous papers (Franchini et al. 2004a, 2004b, hereafter Papers I and II), we selected the stars for the present study on the basis of the two $[\mathrm{Fe/H}]$ catalogs by Taylor (1999, 2003) to ensure overall homogeneity of the analysis and internal consistency. We recall that these catalogs contain F, G, and K stars of luminosity classes II–V and provide mean values of iron metallicity, $[\mathrm{Fe/H}]_{\mathrm{T}}$, and their rms errors (rmse). In order to select stars with supersolar metallicity, we limit the selection to stars with abundance determinations satisfying the following condition: $\mathrm{Diff}_{\mathrm{Fe}} = [\mathrm{Fe/H}]_{\mathrm{T}} - \mathrm{rmse} > 0.0$ dex, with $[\mathrm{Fe/H}]_{\mathrm{T}} > 0.0$ dex.

From the preliminary list of 348 stars satisfying this condition, we excluded those objects for which our analysis may produce uncertain results because of one or more of the following characteristics (according to SIMBAD): variable star, spectroscopic binary, eclipsing binary, double or multiple star, or carbon star.

This selection process led to a list of 242 stars. In order to search for $\alpha$-enhanced stars by means of our method described in Papers I and II, stellar Lick IDS indices (in particular Ca4227, $\mathrm{Mg}_2$, Mg $b$, and Na D) are required. For this study, only a subset of 24 stars is present in the catalog of Lick IDS indices by Worthey et al. (1994, hereafter the Worthey catalog). Therefore, we searched the World Wide Web for extended collections of spectra, allowing us to compute the relevant indices, and the following six spectroscopic stellar libraries were considered:

1. *The STELIB library.*[1]—A homogeneous library of 249 stellar spectra in the visible range 3200–9500 Å, with an intermediate spectral resolution (3 Å; Le Borgne et al. 2003).
2. *The ELODIE library.*[2]—The ELODIE.3 updated release, containing 1962 spectra of 1388 stars taken with the ELODIE spectrograph in the visible range 4000–6800 Å, with a nominal resolution of $R = 10,000$ (Prugniel & Soubiran 2004).
3. *The Nearby Stars Project* (*NBP*) *library.*[3]—A homogeneous library of 216 stellar spectra in the visible range 4840–7000 Å, with a nominal resolution of $R = 60,000$ (Heiter & Luck 2003; Luck & Heiter 2005).
4. *The NStars library.*[4]—A library of 3415 stellar spectra in the visible range 3800–5600 Å, with an intermediate spectral resolution (3.6 Å; Gray et al. 2003); for the sake of homogeneity only NStars Dark Sky Observatory spectra were used.
5. *The Indo-US library.*[5]—A collection of 1273 stellar spectra in the visible range 3460–9464 Å, with an intermediate spectral resolution (1 Å; Valdes et al. 2004).
6. *The S4N (Spectroscopic Survey of Stars in the Solar Neighborhood) database*.[6]—A survey database containing high-resolution ($R \simeq 50{,}000$) spectra for 118 nearby stars in the optical range 3620–9210 Å (AP04).

The six data sets were supplemented by adding the observations of stars with indication of supersolar chemical composition, the Cananea collection, performed by us at the INAOE G. Haro Observatory in Cananea (Mexico) with a Böller & Chivens spectrograph (details in Morossi et al. 2002).

The spectra from the seven data sets, degraded to the Worthey catalog resolution and corrected for radial velocities, have been used to measure the four spectral indices Ca4227, $\mathrm{Mg}_2$, Mg $b$,

[1] STELIB data are available at http://webast.ast.obs-mip.fr/stelib.
[2] ELODIE LL data are available at http://www-obs.univ-lyon1.fr/~prugniel/soubiran.
[3] NBP data are available at http://astrwww.cwru.edu/adam/data.html.
[4] NStars data are available at http://stellar.phys.appstate.edu.
[5] Indo-US data are available at http://www.noao.edu/cflib.
[6] S4N data are available at http://hebe.as.utexas.edu/s4n.

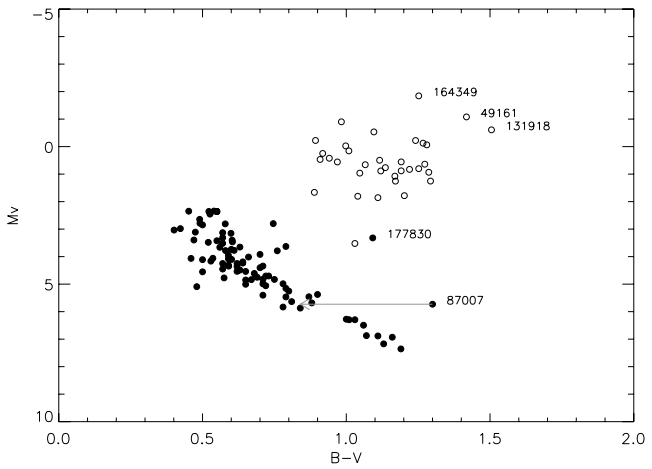


FIG. 1.—$M_V - (B - V)$ color-magnitude diagram. Open and filled circles represent giants and dwarfs, respectively, according to Taylor catalogs. HD 49161, HD 131918, and HD 164349 are classified as supergiants and discarded. HD 87007 has an incorrect $(B - V)$ in SIMBAD, and its correct position according to Kotoneva et al. (2002) is indicated by the arrow. HD 177830, coded as "dwarf" in Taylor catalogs, appears to be, actually, a giant star.

and Na D. For each data set the coefficients to convert its computed indices into the Lick IDS system were derived, via a linear regression technique, by using those stars in common with the Worthey catalog.

For about one-half of the stars in our provisional list, we have at least one complete set of indices either directly from the Worthey catalog or obtained from the data sets listed above. In order to avoid those objects whose surface abundances may not be representative of the initial chemical compositions, we decided to limit the analysis to nonsupergiant stars. This selection was accomplished by looking at the $M_V - (B - V)$ color-magnitude diagram shown in Figure 1 [stellar photometric data, $V$ and $(B - V)$, and parallaxes used to compute $M_V$ are from SIMBAD]. The stars HD 49161, HD 131918, and HD 164349 fall onto the supergiant region of the diagram and therefore were discarded from further analysis leading to a final working set of 119 F-G-K nonsupergiant stars. The distribution of these stars in the eight data sets described above is given in Table 1, and the list of all the program stars is given in Table 2.

The metallicity distribution of the 119 program stars is shown in Figure 2; the middle and bottom panels show, separately, the stars classified as giants (32 objects, including HD 177830) and as dwarfs (87 objects) by Taylor (1999, 2003). The [Fe/H] distributions of the two groups are similar, with the dwarf group extending to higher values than the other group (up to +0.45 dex).

In order to investigate the belonging of our stars to the different Galactic components, we computed their stellar Galactic velocities on the basis of their radial velocities, proper motions, and parallaxes given in SIMBAD. We derived the ($U_{\rm LSR}$, $V_{\rm LSR}$, $W_{\rm LSR}$) velocity components for 115 stars and assembled the corresponding Toomre diagram (Fig. 3). A discrimination between thick- (*filled symbols*) and thin-disk (*open symbols*) stars was attempted by applying the method described in Appendix A by Bensby et al. (2005) and using the 10% normalization factor for the thick-disk star probability.[7] Only one star (HD 145148) appears to belong to the thick disk; nevertheless, its real nature as a thick-disk star is still an open question (see Bensby et al. 2003 and Mishenina et al. 2004). All the other stars are very likely thin-disk stars (101 of which with a high confidence level, $D/TD > 10$). A further check can be done by computing the characteristics of the stellar orbits of the stars present in Figure 3, in particular the mean orbital radius, $R_m$, and the maximum distance from the Galactic plane, $Z_{\rm max}$. We used a code made available to us by J. P. Fulbright (2004, private communication). In the small metallicity range of our sample, Figure 4 does not show a clear radial metallicity gradient in the Galaxy; most of the stars cluster below $Z_{\rm max} = 300$ pc as expected for the thin disk (Nissen 2004). Again, HD 145148 is an outlier with the highest $Z_{\rm max}$. We can conclude that our selection of stars with ${\rm Diff}_{\rm Fe} > 0.0$ dex leads to sample only the thin-disk component of the solar neighborhood.

## 3. SEARCH FOR $\alpha$-ENHANCED STARS VIA INDEX-INDEX DIAGRAMS

In general, detailed high-resolution analysis of individual stars is needed to tackle the problem of determining individual element abundances. In Papers I and II we proposed selected combinations of Lick IDS indices capable of singling out $\alpha$-enhanced stars without requiring previous knowledge of their main atmospheric parameters. On the basis of synthetic spectra (details in Malagnini et al. 2005 and references therein) computed with solar-scaled abundances and enhanced $\alpha$-to-iron ratios (SSA and NSSA grids, respectively),[8] we introduced four combinations of indices, namely, Na D versus Ca4227, Na D versus $Mg_2$, Na D versus Mg $b$, and Na D versus CaMg $= (0.125 \times {\rm Ca4227} + {\rm Mg}_2)$, which allow us to identify different loci in index-index diagrams representative of SSA and NSSA points. Therefore, it is possible to mark a star as either "NSSA" or "SSA" by looking at its position in these diagrams regardless of its effective temperature, surface gravity, and iron abundance by using as a dividing line the lower boundary of the theoretical

[7] A variation of the normalization factor ranging from 6% to 14% does not change the classification.

[8] We recall that our SSA grid is based on Grevesse & Sauval (1998) solar abundances, while the NSSA grid assumes $[\alpha/{\rm Fe}] = +0.4$, where the $\alpha$-elements considered are O, Ne, Mg, Si, S, Ar, Ca, and Ti.

TABLE 1
DISTRIBUTION OF THE 119 PROGRAM STARS IN THE EIGHT DATA SETS

| | Worthey | Cananea | STELIB | ELODIE | NBP | NStars | Indo-US | S4N |
|---|---|---|---|---|---|---|---|---|
| Worthey | 23 | ... | ... | ... | ... | ... | ... | ... |
| Cananea | 9 | 24 | ... | ... | ... | ... | ... | ... |
| STELIB | 5 | 6 | 10 | ... | ... | ... | ... | ... |
| ELODIE | 14 | 10 | 8 | 49 | ... | ... | ... | ... |
| NBP | 11 | 8 | 6 | 23 | 39 | ... | ... | ... |
| NStars | 12 | 10 | 6 | 27 | 25 | 40 | ... | ... |
| Indo-US | 18 | 17 | 9 | 35 | 22 | 29 | 81 | ... |
| S4N | 6 | 4 | 3 | 7 | 8 | 7 | 8 | 12 |

TABLE 2
THE PROGRAM STARS

| HD | Spectral Type | $[Fe/H]_T$ | Error | Code[a] | Worthey | Cananea | STELIB | ELODIE | NBP | NStars | Indo-US | S4N |
|---|---|---|---|---|---|---|---|---|---|---|---|---|
| High-Probability NSSA Stars | | | | | | | | | | | | |
| 50281+..... | K3 V | 0.05 | 0.04 | d | ... | ... | ... | y | y | y | ... | ... |
| High-Probability SSA Stars | | | | | | | | | | | | |
| 7623..... | K2 | 0.17 | 0.09 | g | ... | y | ... | ... | ... | ... | ... | ... |
| 28185..... | G5 | 0.14 | 0.07 | d | ... | ... | ... | ... | y | y | ... | ... |

NOTES.—*Plus sign*: NSSA classification from the Na D vs. Ca4227 diagram only. Table 2 is published in its entirety in the electronic edition of the *Astrophysical Journal*. A portion is shown here for guidance regarding its form and content.
[a] g: giants; d: dwarfs.

SSA locus.[9] This method is quite robust and free from systematic errors due to possible wrong estimates of the stellar $T_{\rm eff}$, log $g$, and [Fe/H] values. The method is particularly suited for analyzing large samples of stars, since it does not require the very demanding and time-consuming observations at high resolution. It has an intrinsic limitation that prevents sound discrimination between SSA and NSSA stars for objects much hotter than the Sun because of the vanishing of the sensitivity to $\alpha$-enhancement due to the clustering of the SSA and NSSA indices at high temperature. Its main range of applicability is therefore for solar-like or cooler stars, and some caution has to be taken to exclude from the analysis supergiant stars, for which atmosphere models are, in general, less reliable. Moreover, it is worth noting that the gain in robustness of our method, due to the choice of not using any estimate of $T_{\rm eff}$, log $g$, and [Fe/H] values, is paid for by an unavoidable reduction in the sensitivity of the Lick IDS indices in discriminating between SSA and NSSA stars. In theory, the SSA or NSSA nature of each star should be assessed by checking whether the distance from the observed point to the corresponding SSA or NSSA theoretical point (i.e., those computed with the proper $T_{\rm eff}$, log $g$, and [Fe/H] values) is within the observational errors. Unfortunately, since the positions of the appropriate theoretical points are unknown, our method must use, as a discriminant, the distance, $d$, of the observed point from the boundary of the whole SSA grid locus. As in Papers I and II, this distance is normalized to the observational errors and defined as $d = [(\Delta_x/\epsilon_x)^2 + (\Delta_y/\epsilon_y)^2]^{1/2}$, where $\Delta_x$, $\Delta_y$ and $\epsilon_x$, $\epsilon_y$ are the $x$- and $y$-differences between the boundary line and the star position and the observational errors of the two indices in each diagram, respectively. Only those stars falling above or below the boundaries at a normalized distance $d > \sqrt{2}$ can be safely identified as "high-probability SSA" or "high-probability NSSA" stars, respectively. If $d > \sqrt{2}$, we cannot confidently classify the stars, and, therefore, we decided to introduce for these objects two categories of uncertain classification (see point 3 below). Unfortunately, the fact that the distance $d$ is measured from the boundary, and not from the actual SSA and NSSA points corresponding to each star, may increase the number of cases with

[9] We do not take into account the upper boundary of the theoretical NSSA points since they were computed by assuming $[\alpha/{\rm Fe}] = +0.4$; therefore, it may not be appropriate in the case of less pronounced $\alpha$-enhancement.

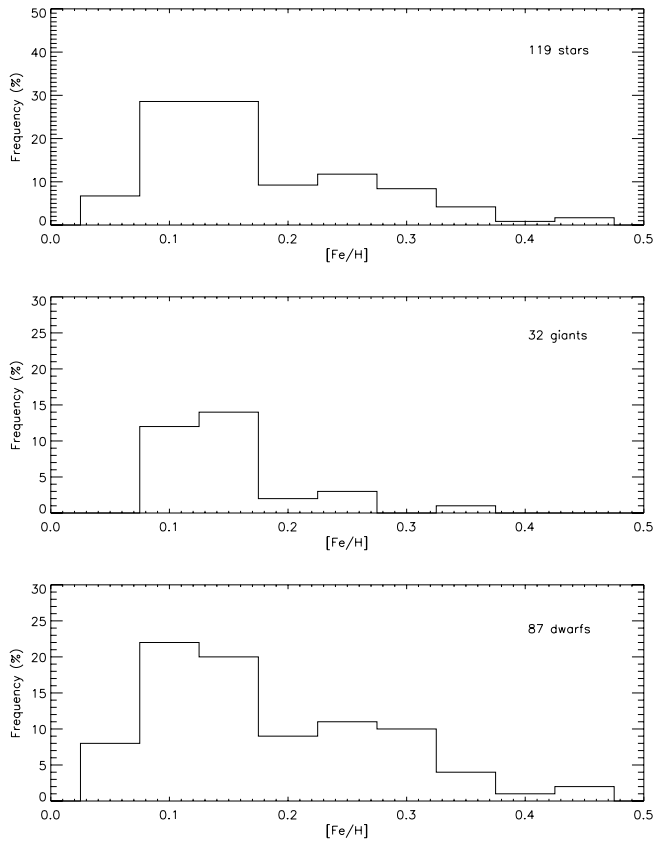


FIG. 2.—[Fe/H] histograms of the total sample (*top*), and of giants (*middle*; HD 177830 is included here; see Fig. 1) and dwarfs (*bottom*), separately.

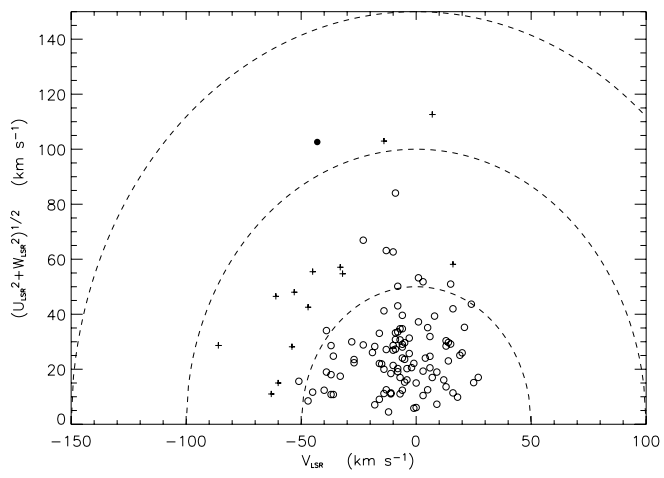


FIG. 3.—Toomre diagram. Thin-disk stars are represented by open circles (higher probability) and crosses (lower probability), while the only thick-disk star, HD 145148, is marked by a filled circle.

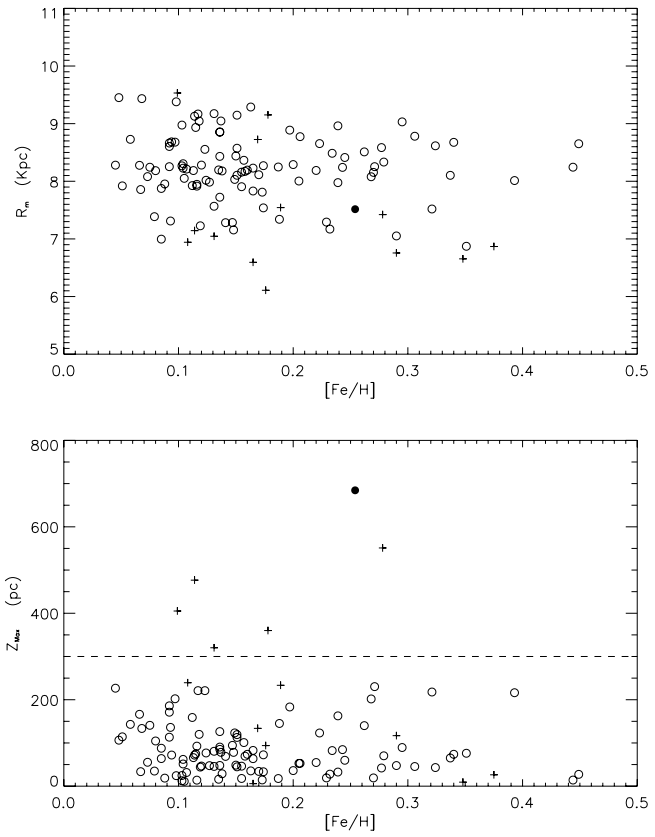


FIG. 4.—Mean galactocentric radius ($R_m$) and maximum distance from the Galactic plane ($Z_{max}$) vs. metallicity (symbols as in Fig. 3).

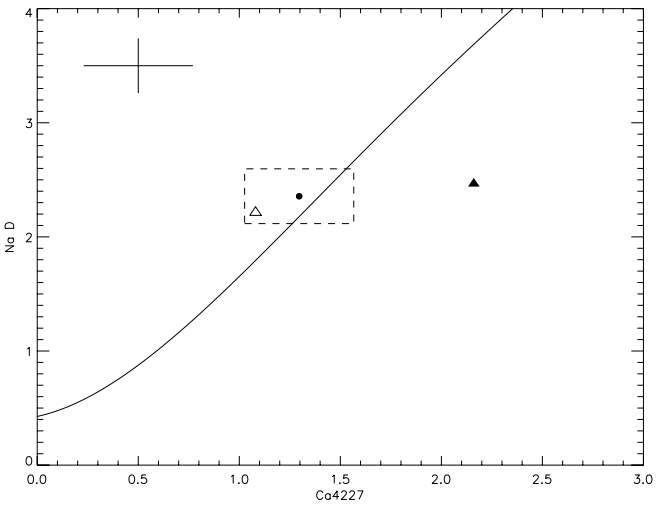


FIG. 5.—Example of uncertain classification because the effective temperature, surface gravity, and metallicity of the analyzed stars are unknown. A simulated observed point (*filled circle*) is plotted together with the corresponding theoretical SSA (*open triangle*) and NSSA (*filled triangle*) points assuming for the simulated star $T_{\rm eff} = 5000$ K, $\log g = 4.5$ dex, and $[{\rm Fe/H}] = -0.5$. The boundary line crosses the observational error box; therefore, the simulated star has an uncertain classification. The star is actually consistent with the SSA point (whose position in real cases is unknown) but, since its distance from the boundary line is less than $\sqrt{2}$, is classified as possible SSA and not as high-probability SSA (see text). The "typical errors per observation of stars" from the Worthey catalog are indicated by a cross in the top left corner.

uncertain classification. In Figure 5 we show a simulated case in which we have to assign an uncertain classification, i.e., "possible SSA," to a star that would be unambiguously classified as high-probability SSA, if we knew its effective temperature, surface gravity, and metallicity and therefore the positions of the corresponding SSA and NSSA theoretical points. The probability of cases like the one depicted in Figure 5 increases, in particular, if the boundaries are drawn to take into account a very large range of possible $T_{\rm eff}$, $\log g$, and [Fe/H] values. Therefore, to increase the effectiveness of our method, we redefined in this paper the boundary lines of Papers I and II, which were based on the position of all the SSA grid points irrespective of their [Fe/H] values, by using only those SSA points with $[{\rm Fe/H}] > -0.5$ dex. In fact, in this paper we deal with stars with nominal $[{\rm Fe/H}] > 0.0$ dex.[10] Moreover, to increase the statistical accuracy of the measured indices, we averaged individual values from all the available data sets (see Table 2). Figure 6 shows, for each index, the distribution of the standard errors of the derived mean values together with, as a reference, the corresponding "typical error per observation of stars," $\epsilon$, reported in Table 1 of the Worthey catalog (we recall that $Mg_2$ is given in magnitudes, while Ca4227, Mg *b*, and Na D are in Å). In general, the standard errors are consistent with the $\epsilon$ values, except for $Mg_2$, suggesting that the uncertainty reported in the Worthey catalog for this index may be underestimated. In the computation of the distances the observational error associated with each index is the maximum between the value listed in the Worthey catalog and the standard error (Worthey catalog values were used for stars present in only one data set).

Figure 7 shows the positions of our stars in the four index-index diagrams used to identify the $\alpha$-enhanced candidates in our sample. The main derived results are as follows:

1. The absence of any high-probability NSSA star, thus well below the boundary line ($d > \sqrt{2}$) in at least one diagram, with the only exception of HD 50281 (*filled triangle*).
2. The identification of 38 high-probability SSA stars (*filled circles*) obtained by picking up those well above the boundary lines ($d > \sqrt{2}$) in all the Na D versus Ca4227, Na D versus $Mg_2$, and Na D versus CaMg diagrams.[11]
3. The presence of 80 stars too close to the boundary lines to draw any sound conclusion. Actually, we cannot classify as NSSA or SSA any of the 35 star with $(B - V) < 0.6$ because of the loss of sensitivity of our method at high temperatures due to the coalescence and vanishing of the observed and synthetic indices. In the remaining 45 cases we divided the stars into two groups according to their position with respect to the boundary lines. The 38 stars above the boundary lines in Figures 7*a*, 7*b*, and 7*d* may have some chance of having solar-scaled composition and are classified as possible SSA objects; on the contrary, the remaining seven stars, which fall below the boundary in at least one of the panels in Figure 7, may have some chance of being $\alpha$-enhanced and are classified as "possible NSSA" objects.

### 3.1. *High-Probability and Possible NSSA Stars*

The only star classified as a high-probability NSSA, HD 50281, deserves some discussion. First of all, we remark that its nature of supersolar star is doubtful. In fact, quite different iron metallicity estimates are reported in the literature: $[{\rm Fe/H}] = 0.05 \pm 0.04$ in Taylor (2003), but $[{\rm Fe/H}] = -0.20 \pm 0.10$, $[{\rm Fe/H}] = 0.06 \pm 0.09$, and $[{\rm Fe/H}] = -0.04 \pm 0.07$ in Mishenina et al. (2004),

[10] We confidently assume that the metallicity values from Taylor (1999, 2003) cannot be wrong by more than 0.5 dex.

[11] The Na D vs. Mg *b* diagram is not suitable to this purpose, as can be seen in Fig. 7*c* of Paper I.

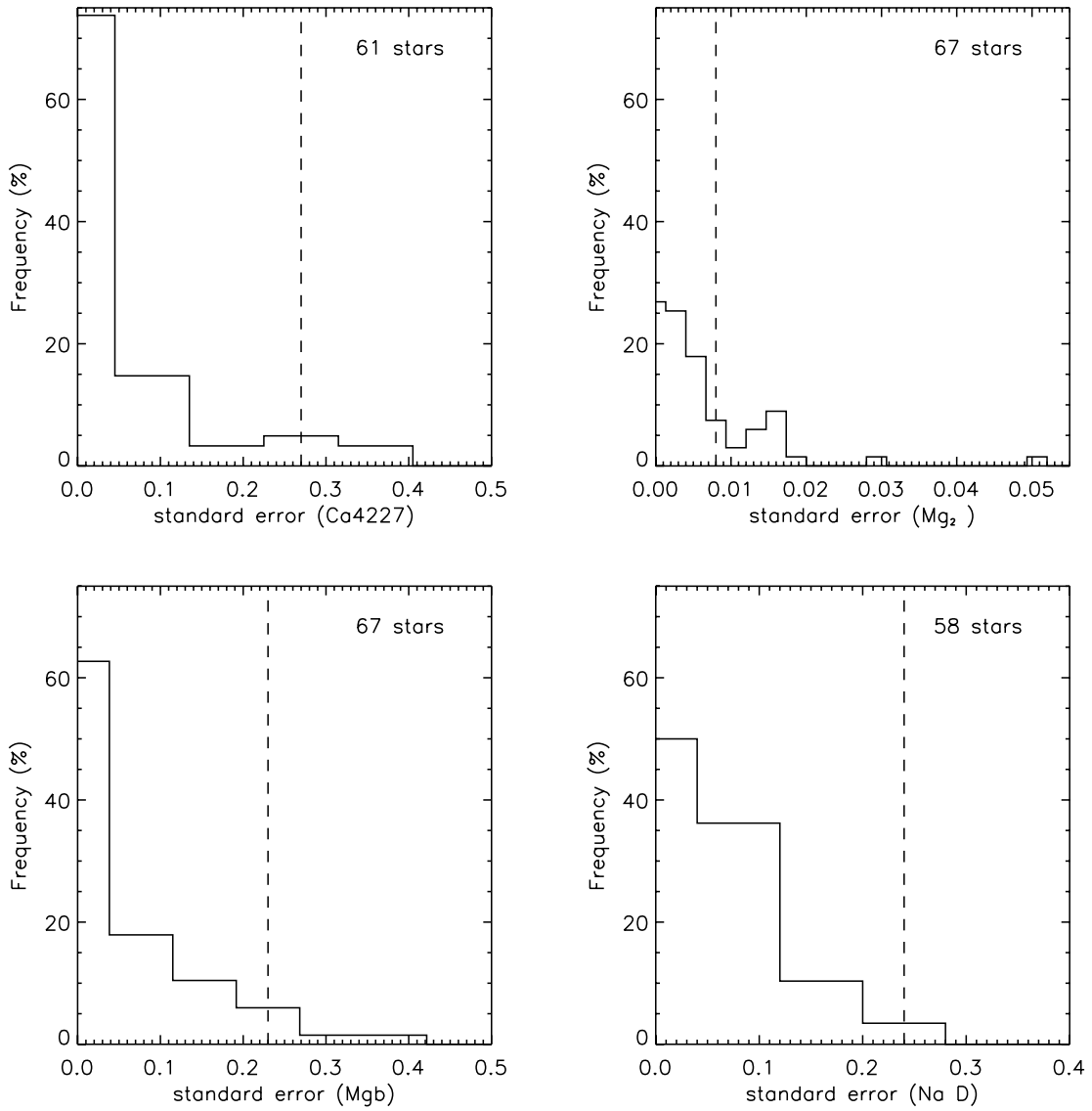


FIG. 6.—Comparison of distributions of index standard errors with the corresponding observational errors (*dashed vertical lines*) from the Worthey catalog. The largest value in the $Mg_2$ diagram is due to anomalous differences in the index values computed from the different spectra of HD 136834.

Luck & Heiter (2005), and Beirão et al. (2005), respectively. As far as our classification is concerned, we note that the star falls below our boundary lines only in the diagrams based on the Ca4227 index. Its positions in the $Mg_2$ and Mg $b$ diagrams do not indicate any Mg enhancement; therefore, the star seems to be more likely a Ca overabundant object than a real $\alpha$-enhanced one. A self-consistent analysis of HiRes spectra of the same kind as that described in § 4.5 is in progress, and preliminary results indicate that our detection may be spurious because of the relatively poor quality of the stellar spectra in the region below 4400 Å. In fact, its spectrum from the ELODIE library, which is the only available in the Ca4227 index region, shows hints of a nonoptimal correction of the spectral order blaze function that may have affected our computation of the index.

As far as the seven possible NSSA stars are concerned, four of them fall below boundary lines in only one diagram and at very small normalized distances ($d < 0.4$, i.e., $d \ll \sqrt{2}$). Of the remaining three stars, HD 119291 is probably the coolest object in our sample, as suggested by its spectral classification and very high Na D index value. We cannot exclude that its $T_{\rm eff}$ could be close to or even below the lower limit of our theoretical grid where the reliability of synthetic indices is lower. The other two stars, HD 20512 and HD 17382, fall below the boundaries in more than one diagram, with maximum normalized distances $d = 0.90$ (in the $Mg_2$ diagram) and $d = 0.77$ (in the CaMg diagram), respectively. We must point out that both stars are listed as long-period spectroscopic binaries by Latham et al. (2002; even if SIMBAD classifies them simply as high proper-motion stars; therefore, they were kept in our sample), thus suggesting the possibility of some contamination by a companion star in their index values. In conclusion, we can say that our choice of classifying these seven objects as possible NSSA stars is very conservative. In any case we maintain this classification in the following sections to be sure to avoid the risk of losing candidate $\alpha$-enhanced stars because of possible overestimates of observational errors and/or small uncertainties in the definition of the boundary lines. We must, in fact, recall that we obtained our theoretical index values, and therefore the position of the boundaries, via a calibration of the computed synthetic indices to the Lick IDS system. This calibration was performed by matching, via a linear correlation, synthetic and observed (Worthey catalog) indices for a set of stars with atmospheric parameters given in Thevenin

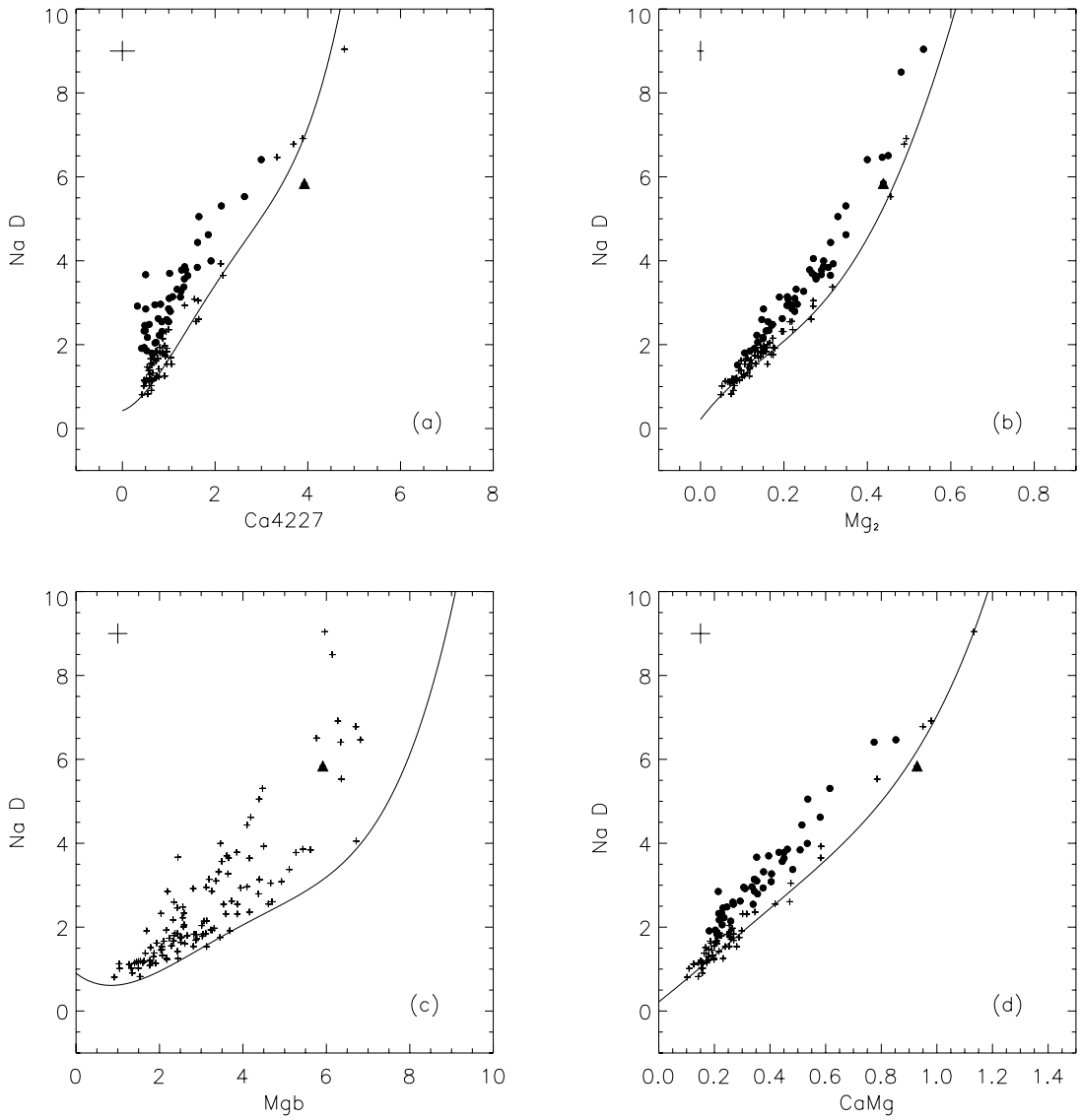


FIG. 7.—Index-index classification diagrams. Filled circles represent high-probability SSA stars, crosses show the nonclassifiable stars or possible SSA and possible NSSA stars, and the filled triangle indicates HD 50281 (see text). The lines represent the lower boundaries of the theoretical SSA points with $[Fe/H] > -0.5$ dex.

(1998).[12] As a consequence, the precision in the position of the boundaries in Figure 7 depends on the effectiveness of the least-squares fitting in washing out the uncertainties in the Worthey observations and in the Thevenin parameters of the calibration stars. A check on the stability of the calibration coefficients performed by using more recent atmospheric parameters (Fuhrmann 2004; Mishenina et al. 2004) than those from Thevenin led to new values that agree with those derived in Paper I within the estimated standard errors. To ensure consistency and an easier comparison of the results, the same calibration as that in Papers I and II has been used in this paper.

Table 2 lists all 119 stars grouped in five different sections according to our classification scheme. In conclusion, our classification indicates that $\alpha$-enhanced stars are very rare in our sample of supersolar metallicity thin-disk stars. Actually, the percentage of NSSA candidates over the 84 classified stars is about 1%, and even if, to be very conservative, we take into account also all the possible NSSA stars, it does not exceed 10%. As far as the 35 unclassified stars are concerned, we expect similar percentages. In fact, they span almost the same [Fe/H] range of values and show the same kinematical properties as the classified ones. Moreover, they are all *hot* main-sequence stars, with an age equal to or slightly lower than the other stars. It is therefore very unlikely that the percentage of $\alpha$-enhanced stars among them would differ significantly from those derived by looking at the classified stars.

[12] Vizier Online Data Catalog, III/193 (F. Thevenin, 1998).

## 4. OUR RESULTS AND THE CURRENT SCENARIO FROM HIGH-RESOLUTION SPECTROSCOPY

In this section we compare our results with those from several studies based on high-resolution spectroscopy to understand whether the low percentage of NSSA candidates found in § 3 is an intrinsic characteristic of the whole population of supersolar stars or if it is specific to only the stars in our sample.

In recent years many papers report individual abundance determinations of $\alpha$-elements derived from the analysis of high-resolution spectra. From among the impressive number of papers, in particular for solar neighborhood stars, we hereafter use four of them (and references therein) to discuss and compare our results.

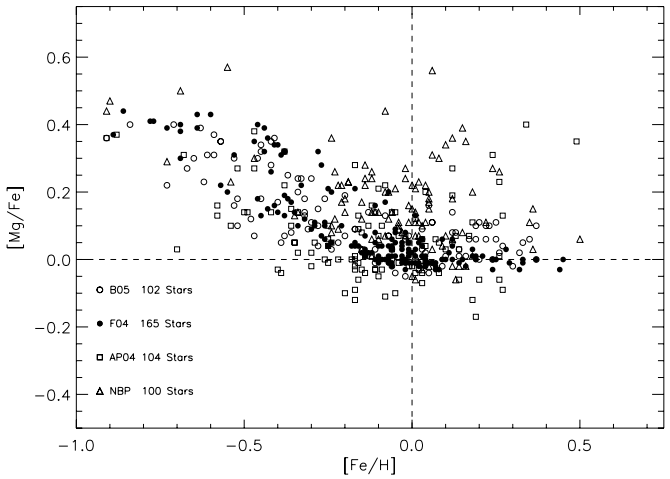


FIG. 8.—Abundance ratio [Mg/Fe] vs. [Fe/H] from the four different sources listed in the bottom left corner (see text).

The four papers, AP04, Fuhrmann (2004, hereafter F04), Bensby et al. (2005, hereafter B05), and Luck & Heiter (2005, hereafter LH05), are all based on homogeneous analysis of large samples of stars. In particular, we focus our attention on the trend of magnesium, measured by [Mg/Fe], in high-metallicity Galactic disk stars as representative of the behavior of $\alpha$-elements.

In spite of different proportions of thin- and thick-disk stars in the samples studied in the aforementioned papers, all of them agree in finding a different behavior for the two Galactic disk components. In fact, the thick-disk stars are characterized by higher values of [Mg/Fe] at a given [Fe/H] with respect to the thin-disk ones and show a decrease from $[\mathrm{Mg/Fe}] = +0.4$ for $[\mathrm{Fe/H}] < -1.0$ to $[\mathrm{Mg/Fe}] \sim 0.0$ at $[\mathrm{Fe/H}] = 0.0$, in agreement with predictions by current nucleosynthesis theories and Galactic chemical evolution models (e.g., Matteucci 2004). As far as the thin-disk stars are concerned, all the papers show a gentle decrease of [Mg/Fe] abundance ratios for [Fe/H] increasing from its lower limit at about $-0.8$ dex up to 0.0 dex. The situation is much more in debate in the metallicity range we are interested in. In particular, AP04 claim the presence of an increase of [Mg/Fe] at supersolar regime. This result contradicts the findings of F04, who found a plateau at about $[\mathrm{Mg/Fe}] = 0.0$ for $[\mathrm{Fe/H}] > 0.0$ dex. Similarly to F04, B05 found a plateau at high metallicities, but with a small offset of about +0.05 dex. On the other hand, quite a large scatter is present in LH05 data, thus hampering the detection of any trend.

In order to summarize the observational picture, we overplot in Figure 8 the results for $[\mathrm{Fe/H}] > -1.0$ from the four reference papers. Quite a large spread is visible, which is partly intrinsic because of the copresence of thin- and thick-disk stars and partly due to internal and external errors. The first cause of spread should be less effective for $[\mathrm{Fe/H}] > 0.0$, since the large majority of stars in this metallicity range is expected to belong to the thin-disk component. In order to get better insight into the differences among different authors, in Figure 9 we analyze the results for the stars in common in two data sets at a time. The comparison between B05 and LH05 is limited to four stars only, but even this case supports a general conclusion about LH05 results:

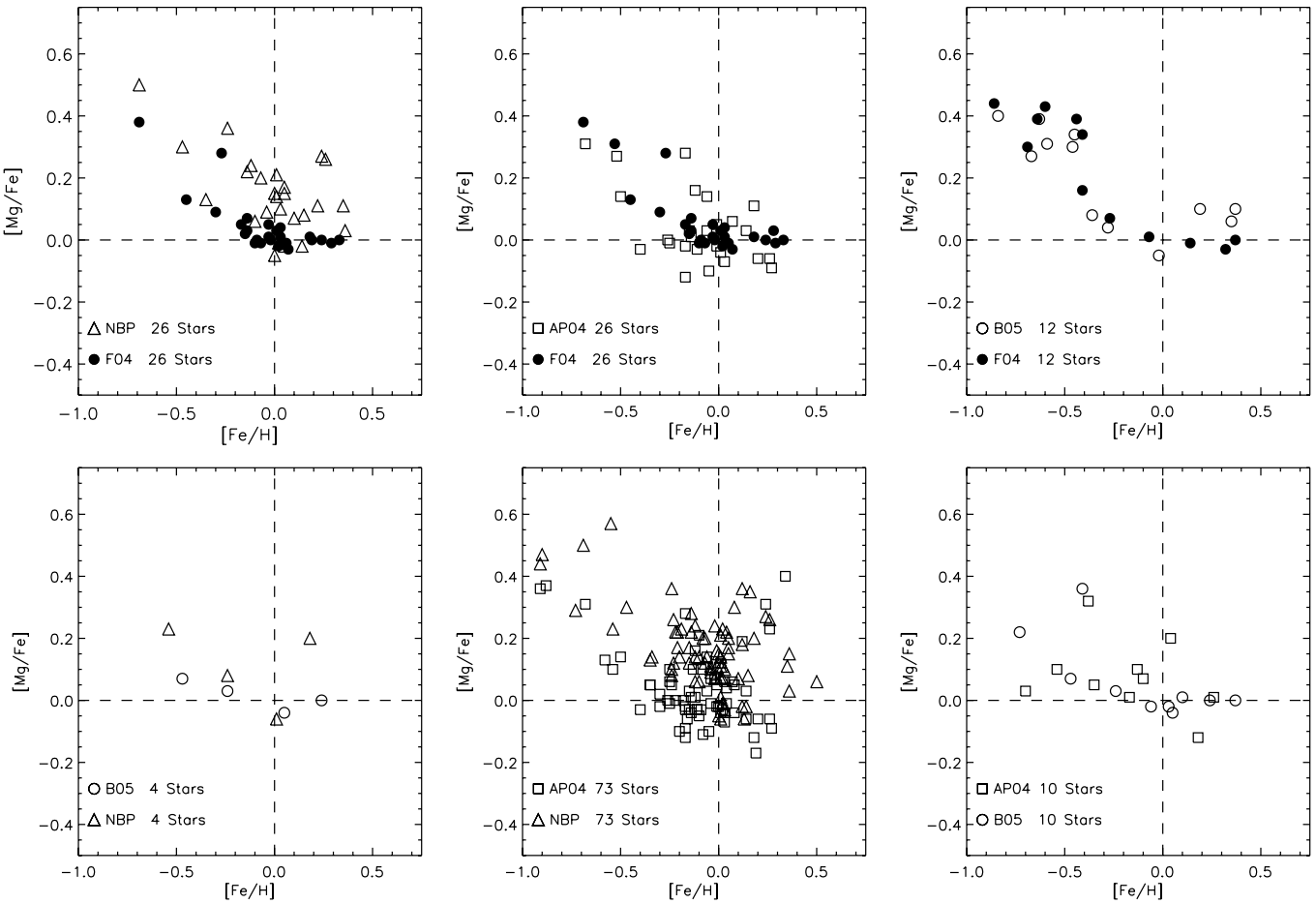


FIG. 9.—Comparison of [Mg/Fe] vs. [Fe/H] for stars present in two sources at a time.

TABLE 3
PERCENTAGES OF $\mathrm{Diff_{Mg}} > 0.0$ AND NSSA OBJECTS IN DIFFERENT SAMPLES OF SUPERSOLAR STARS

| | | | Stars Reanalyzed in This Paper | | |
|---|---|---|---|---|---|
| Sample | Number of Supersolar Stars | Percentage of $\mathrm{Diff_{Mg}} > 0.0$ Stars | Number of Supersolar Stars | Percentage of $\mathrm{Diff_{Mg}} > 0.0$ Stars | Percentage of NSSA Stars |
| AP04 ..... | 11 | 55 | 10 | 60 | 0 (10) |
| F04 ..... | 22 | 5 | 15 | 7 | 0 (27) |
| B05 ..... | 22 | 14 | 8 | 25 | 0 (0) |
| LH05 ..... | 14 | 36 | 9 | 33 | 0 (22) |
| Our sample..... | 84 | 1 (10) | | | |

NOTES.—Conservative estimate percentages computed counting also possible NSSA stars are given in parentheses.

[Mg/Fe] ratios in LH05 are generally higher than those given in the other papers at about the same [Fe/H] values. To a lesser extent, AP04 results show a behavior similar to that of LH05. AP04 and LH05 have the maximum number of stars in common (73) and show quite a large scatter between their results. The comparison in the case of B05 data is limited to smaller samples and shows a reasonably good agreement with F04.

A complete and thorough analysis of the causes of the discrepancies shown in Figures 8 and 9 is beyond the aim of this paper; therefore, in the following, we compare our results with those from each paper individually. The comparison is made by taking into account from each of the four samples those stars that satisfy the same condition at the base of the selection of our sample, i.e., $\mathrm{Diff_{Fe}} > 0.0$ dex, where the [Fe/H] and their rmse values are taken from the corresponding paper. Furthermore, the constraints listed in § 2 are applied. In Table 3 we report the number of supersolar stars in each sample, together with the percentages of $\alpha$-enhanced ones according to the different authors. The conditions to consider a star as $\alpha$-enhanced are $[\mathrm{Mg/Fe}] > 0$ and $\mathrm{Diff_{Mg}} = [\mathrm{Mg/Fe}] - \mathrm{rmse} > 0.0$ dex.

As can be seen, the percentages of $\mathrm{Diff_{Mg}} > 0.0$ dex stars in F04 and B05 are comparable to the conservative percentage estimated of NSSA stars in our sample (10%). On the contrary, the AP04 and LH05 samples show much larger percentages of $\alpha$-enhanced stars than those found by F04, B05, and in our sample. Furthermore, we note that, as already shown in Figure 9, different authors may give different classification of the same star; for instance, of the six stars in common between AP04 and LH05, only two have concordant classification. In an attempt to reduce the effects of the different assumptions and analysis techniques used by AP04, F04, B05, and LH05, we reclassify as many as possible of their supersolar stars by applying our method. With this aim we searched our data sets for spectra of the AP04, F04, B05, and LH05 supersolar stars with $(B - V) > 0.6$ (see § 3). The list of the 33 stars found is given in Table 4; we recall that the stars classified as supersolar according to Taylor (1999, 2003) are already present in our sample (Table 2). The second part of Table 3 reports the actual numbers of stars for which we can perform the comparison of the percentages given by the various $\mathrm{Diff_{Mg}}$ estimates with those from our classification. In the following we discuss in detail the results for each individual sample.

### 4.1. *The AP04 Sample*

The index-index diagrams in Figure 10 show the positions of the subset of supersolar stars from AP04. By combining the outcome of the four panels, we classify the 10 stars as follows: three stars as high-probability SSAs, six stars as possible SSAs, and only one as a possible NSSA. Thus, no high-probability NSSA star seems to be present. If we want to be conservative and count the possible NSSAs, we obtain a percentage of 10%, a value that is much lower than that obtained from AP04 $\mathrm{Diff_{Mg}}$ estimates (see the second part of Table 3 and Fig. 15*a*). Moreover, our conservative percentage could even be overestimated if we note that the only possible NSSA star may not be a real supersolar one because of a discrepancy between AP04 ($[\mathrm{Fe/H}]_{\mathrm{AP04}} - \mathrm{rmse} = +0.04$) and Taylor (1999, 2003) ($[\mathrm{Fe/H}]_{\mathrm{T}}$-rmse $= -0.08$) estimates of metallicity. As far as the six AP04 stars with $\mathrm{Diff_{Mg}} > 0.0$ are concerned, we classify four of them as possible SSAs and the remaining two as high-probability SSAs.

As already discussed in FR05, AP04 results may be affected by an underestimate of the $T_{\mathrm{eff}}$ values used in their analysis, which produces an overestimate of [Mg/Fe]. In Figure 11 we show, as an example, the dependence of the derived abundance ratios on a variation of 100 K in the adopted $T_{\mathrm{eff}}$ as computed from the data in Table 5 of AP04 (solid lines indicate the average trends). As can be seen, this increase in temperature introduces variations in the element abundance ratios [Fe/H] and [Mg/Fe] as large as 0.1 dex, thus showing the importance of using very accurate values of $T_{\mathrm{eff}}$ in deriving $[\alpha/\mathrm{Fe}]$ ratios. Moreover, it is worth noting that the abundance variations in Table 5 of AP04 probably do not take into account that a variation in the adopted effective temperature should also imply a redetermination of the value of surface gravity and that this fact may introduce a second-order effect. Note the presence of a quite large scatter in Figure 11 in the [Mg/Fe] diagram for temperatures below 5500 K, which indicates a not unique dependence of this ratio on the accuracy of the assumed $T_{\mathrm{eff}}$.

### 4.2. *The F04 Sample*

The index-index diagrams in Figure 12 show the positions of the subset of supersolar stars from F04. By combining the outcome of the four panels, we classify the 15 stars as follows: three stars as high-probability SSAs, eight stars as possible SSAs, and four stars as possible NSSAs. As in the previous section, no high-probability NSSA star is found; in this case the conservative percentage of NSSA stars is 27% (see second part of Table 3 and Fig. 15*b*). As far as the only F04 star with $\mathrm{Diff_{Mg}} > 0.0$ is concerned, we classify it as a possible NSSA.

### 4.3. *The B05 Sample*

The index-index diagrams in Figure 13 show the positions of the subset of supersolar stars from B05. By combining the outcome of the four panels, we classify all eight stars as possible SSAs. In this case even the conservative percentage of NSSA stars is zero (see the second part of Table 3 and Fig. 15*c*). We are in agreement with B05 in classifying six stars as SSAs, while we do not confirm the nature of NSSA stars for the remaining

TABLE 4

CLASSIFICATION OF AP04, F04, B05, AND LH05 SUPERSOLAR STARS

| | T | | | AP04 | | | F04 | | | B05 | | | LH05 | | |
|---|---|---|---|---|---|---|---|---|---|---|---|---|---|---|---|
| HD | [Fe/H] | rmse | $Diff_{Fe}$ | [Fe/H] | rmse | $Diff_{Fe}$ | [Fe/H] | rmse | $Diff_{Fe}$ | [Fe/H] | rmse | $Diff_{Fe}$ | [Fe/H] | rmse | $Diff_{Fe}$ |
| 9562..... | 0.11 | 0.05 | 0.06 | ... | ... | ... | ..... | ... | ... | 0.20 | 0.10 | 0.10 | ... | ... | ... |
| 10780..... | 0.10 | 0.06 | 0.05 | ... | ... | ... | ... | ... | ... | ... | ... | ... | 0.07 | 0.06 | 0.01 |
| 32147..... | 0.29 | 0.03 | 0.26 | 0.26 | 0.05 | 0.21 | ... | ... | ... | ... | ... | ... | 0.38 | 0.10 | 0.28 |

| | AP04 | | | F04 | | | B05 | | | LH05 | | | |
|---|---|---|---|---|---|---|---|---|---|---|---|---|---|
| | [Mg/Fe] | rmse | $Diff_{Mg}$ | [ Mg/Fe] | rmse | $Diff_{Mg}$ | [ Mg/Fe] | rmse | $Diff_{Mg}$ | [ Mg/Fe] | rmse | $Diff_{Mg}$ | CLASSIFICATION |
| 9562..... | ... | ... | ... | ... | ... | ... | 0.11 | 0.10 | 0.01 | ... | ... | ... | SSA |
| 10780..... | ... | ... | ... | ... | ... | ... | ... | ... | ... | 0.06 | 0.06 | 0.00 | NSSA |
| 32147..... | 0.23 | 0.09 | 0.14 | ... | ... | ... | ... | ... | ... | 0.13 | 0.17 | −0.04 | SSA |

NOTES.—Table 4 is published in its entirety in the electronic edition of the *Astrophysical Journal*. A portion is shown here for guidance regarding its form and content.

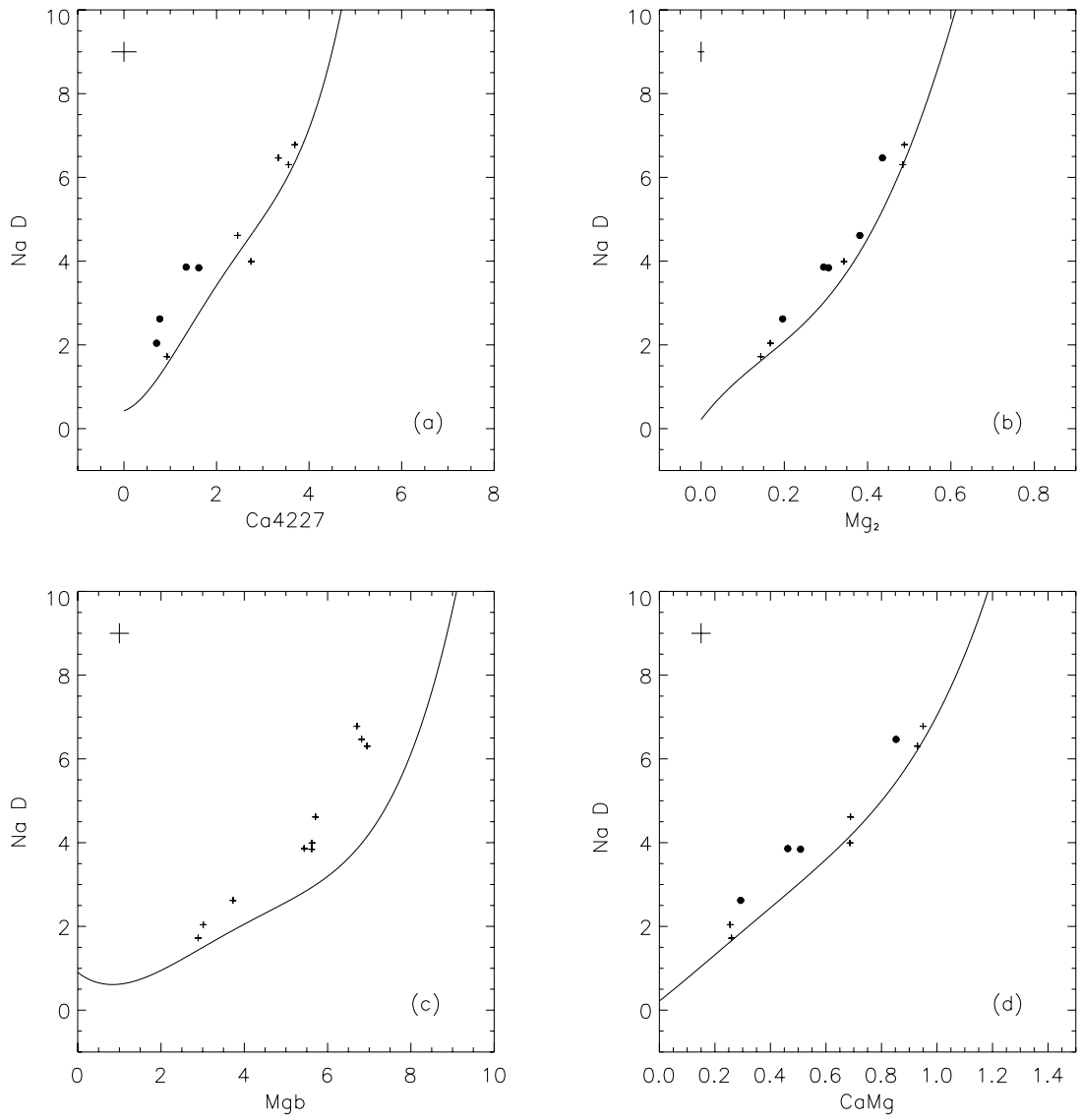


FIG. 10.—Index-index classification diagrams for supersolar stars in AP04. Filled circles represent high-probability SSA stars, and crosses indicate possible SSA or possible NSSA stars. The lines represent the lower boundaries of the theoretical SSA points with [Fe/H] > −0.5 dex.

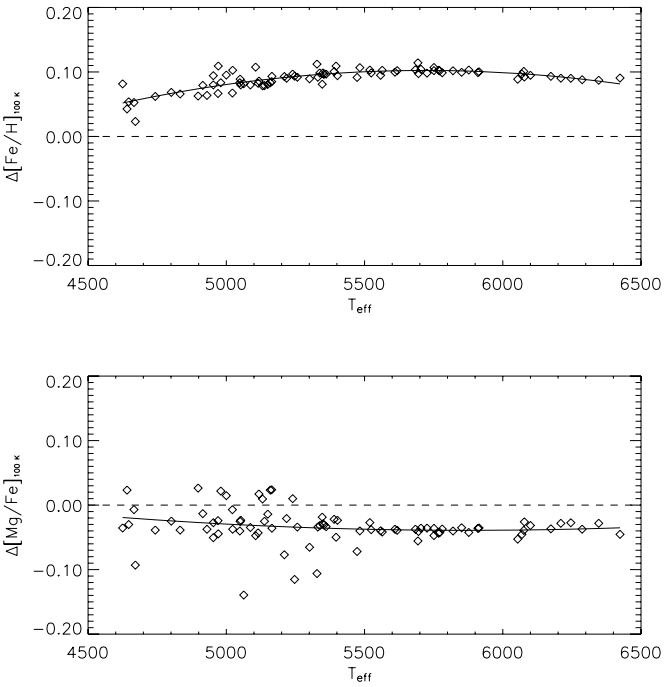


FIG. 11.—Variations of AP04 [Fe/H] and AP04 [Mg/Fe] per an increase of 100 K at different $T_{\rm eff}$ values.

two objects with $\mathrm{Diff}_{\rm Mg} > 0.0$, since we classify them as possible SSAs. We note that for both these objects $\mathrm{Diff}_{\rm Mg}$ is only 0.01 dex; therefore, the $\alpha$-enhancement derived by B05 should be taken with caution.

### 4.4. *The LH05 Sample*

The index-index diagrams in Figure 14 show the positions of the subset of supersolar stars from LH05. By combining the outcome of the four panels we classify the nine stars as follows: three stars as high-probability SSAs, four stars as possible SSAs, and two stars as possible NSSAs. Also in this case no high-probability NSSA star is found; the conservative percentage of NSSA stars is 22% and is much lower than that obtained from LH05 $\mathrm{Diff}_{\rm Mg}$ values (see the second part of Table 3 and Fig. 15*d*). As far as the three LH05 stars with $\mathrm{Diff}_{\rm Mg} > 0.0$ are concerned, we classify them as possible SSAs.

The comparison of our classification results with AP04, F04, B05, and LH05 are given in Table 4.

### 4.5. *The Extreme Case of HD 125072*

This star, as can be seen in Table 4 and in Figure 15, has the highest [Fe/H] and a very high [Mg/Fe] according to AP04. Its nature of supersolar star is confirmed by looking at [Fe/H] in Taylor (2003), but our classification procedure does not find any trace of $\alpha$-enhancement, even if our results are based on indices computed from the same spectrum used in AP04 analysis.

As a possible explanation of this discrepancy, we recall that abundance ratios are not directly observable quantities. They must be derived from observational quantities (i.e., equivalent widths) through stellar atmosphere models, and the reliability of the derivation process depends strongly on the accuracy of the main atmospheric parameters, namely, $T_{\rm eff}$, $\log g$, and the chemical composition adopted in the analysis. In particular, the determination of the most important parameter, $T_{\rm eff}$, in F, G, and K stars is not straightforward due to difficulties in finding a unique value that satisfactorily reproduces the observed photometry and, at the same time, provides the correct ionization balance of neutral and first ionized elements (see discussion in AP04 and in Melendez & Ramirez 2005). In particular, AP04 found for this star [Fe/H] = +0.5 and +1.0 from Fe I and Fe II, respectively, and had difficulties in deriving consistent abundances from Ca I and Ca II (see Fig. 9 in AP04).

We must also stress the importance of using fully consistent atmosphere model structures in the analysis of high-resolution spectra for deriving elemental abundances. Bonifacio & Caffau (2003) showed that the stellar atmosphere structure of cool stars is very sensitive to the $\alpha$-element abundances, in particular to [Mg/H], since magnesium is one of the main electron donors (Sbordone et al. 2005). In fact, while the Fe abundance plays a main role in determining the atmosphere temperature structure via line blanketing, the electron pressure structure and the $H^-$ opacity are significantly affected by the Mg abundance. Therefore, to avoid systematic errors as large as 0.20 dex in the derived Mg abundance, it is mandatory to use atmosphere models computed with self-consistent abundance patterns.

Following the above-given prescriptions, we undertook a new high-resolution analysis based on the use of Kurucz ATLAS9, ATLAS12, and SYNTHE codes for computing atmosphere models and synthetic spectra and deriving detailed chemical abundances. While the ATLAS9 code computes models only for a set of abundances fixed by the adopted opacity distribution functions (ODFs), the ATLAS12 code handles the line blanketing with the opacity sampling method, and therefore it is able to compute models with arbitrary chemical composition. Atomic and molecular line lists from the Kurucz database provide the basis of the line data after the following modifications and implementations: (1) replacement of several theoretical log $gf$ with astrophysical values derived from the comparison of the solar synthetic spectrum with the Solar Flux Atlas from Kurucz et al. (1984); (2) addition of hyperfine and isotopic components for a few lines of Sc I, V I, Mn I, Co I, Cu I, Ba II, and Eu II; (3) inclusion of a large number of Van der Waals broadening constants from Barklem et al. (2000); (4) modification of the SYNTHE code to allow for the dependence of the Van der Waals broadening on temperature according to the Anstee & O' Mara (1995) theory.

The initial step needed to obtain the starting atmosphere model for the K3 V star HD 125072 and the procedure needed to derive its elemental abundances are described below. It differs from the high-resolution analysis usually adopted in the literature because it requires a complete self-consistency between the derived abundances and those used in the computation of the stellar atmosphere structure.

#### 4.5.1. *Observational Data and Initial Model*

The observed spectrum of HD 125072 is the same used by AP04 and was downloaded from the S4N archive. It was observed at ESO with the FEROS spectrograph in the 3620–9210 Å range at a resolving power of about 45,000.

The initial model parameters, $T_{\rm eff}$, $\log g$, and [M/H][13] were determined from the comparison of observed $(B-V)$ and $(V-I)_{\rm C}$ (Cousins) indices with synthetic indices computed for [M/H] = 0.0, +0.2, and +0.5. The observed indices, $(B-V) = 1.017$ and $(V-I)_{\rm C} = 1.02$, were taken from the *Hipparcos* Catalog. The adopted synthetic photometry is similar to that described by Castelli (1999) and Bessell et al. (1998) but for the use of NEWODF ATLAS9 models (Castelli & Kurucz, 2003). We assumed as starting $T_{\rm eff}$ and [M/H] those reproducing both

[13] A solar-scaled chemical composition is assumed as a starting point.

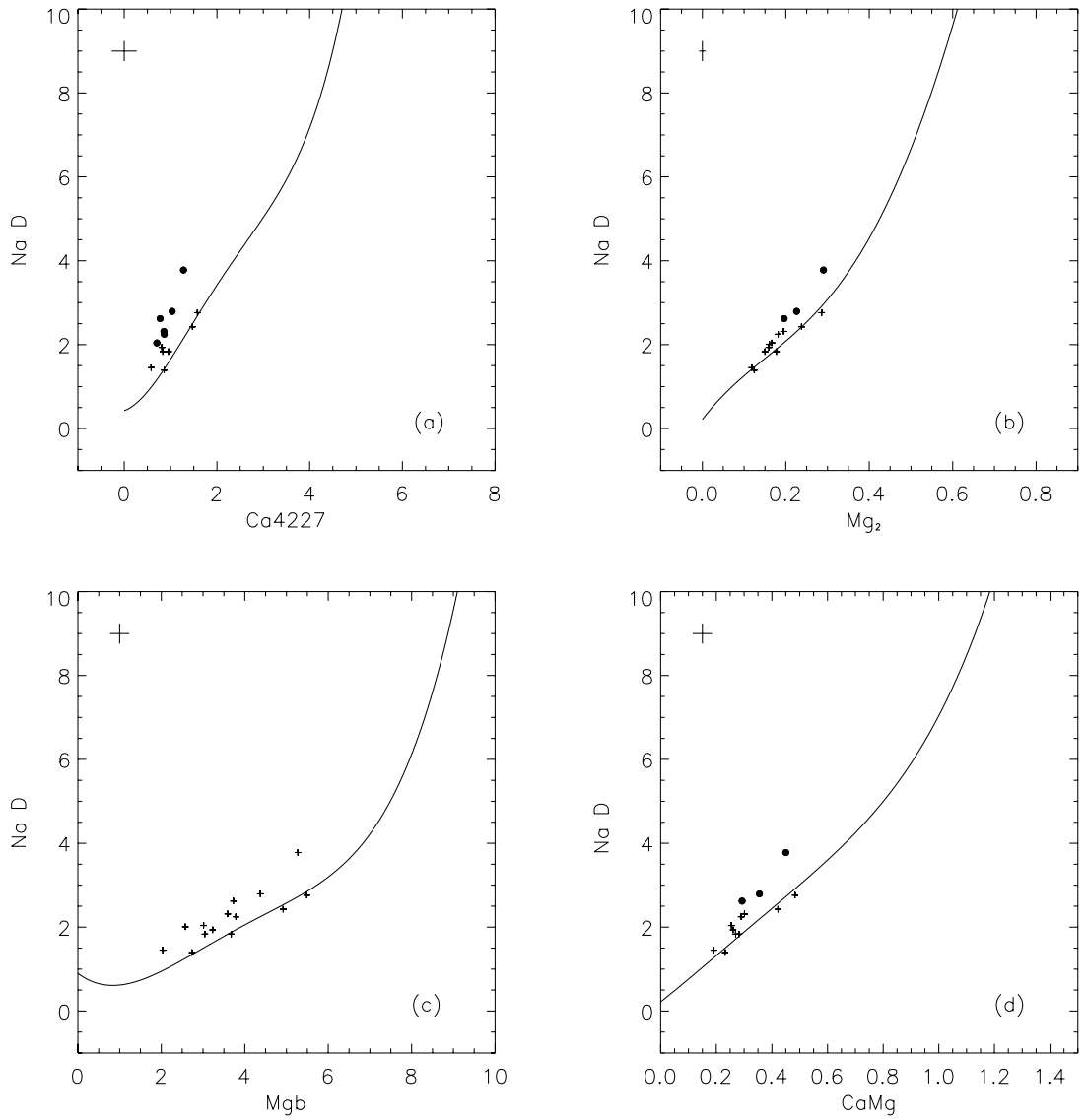


FIG. 12.—Index-index classification diagrams for supersolar stars in F04 (symbols and boundary lines as in Fig. 10).

indices for $\log g = 4.5$. The $\log g$ value was adopted according to the stellar luminosity class, and in any case we recall that $(B - V)$ and $(V - I)_C$ color indices are almost independent of gravity for G–K dwarfs. Initial $T_{\rm eff}$, $\log g$, and [M/H] are given in Table 5. We assumed $\xi = 1$ km s$^{-1}$ for the microturbulent velocity. The synthetic spectra were broadened for a Gaussian instrumental profile, $R = 45{,}000$, corresponding to the ESO FEROS spectrograph nominal resolving power and a rotational velocity $v \sin i = 2$ km s$^{-1}$.

#### 4.5.2. *Abundance Determination Procedure*

First of all, a synthetic spectrum with the above-derived initial parameter values is computed to perform a comparison with the observed one in the regions of Ca II 8662 Å, Ca I 6162.173 Å, Mg I 5528.405 Å, and Fe I 5232.405 Å. Then the model parameter values and the individual elemental abundances are checked and refined (if needed) by applying the following procedure:

1. The Ca II line is used to derive the calcium abundance since its wings are almost independent of both $T_{\rm eff}$ and $\log g$ in cool dwarfs (Chmielewski 2000). The Ca I line at 6162.173 Å is used to fix the gravity once the Ca abundance is known. Everything is checked by looking at the Ca I triplet lines at 6102, 6122, and 6162 Å, which are good luminosity indicators (Cayrel et al. 1996).

2. A new trial model is computed with ATLAS12 with the new gravity and Ca abundance (we note that this new model has no more solar-scaled chemical composition). The new synthetic spectrum is used to determine the Mg and Fe abundances by comparing the observed and computed profiles of Mg I at 5528.405 Å and Fe I at 5232.405 Å.

3. The so-obtained Mg and Fe abundances, if different from those assumed in the trial model, are used to compute a new atmosphere model and to recompute the Ca I and Ca II profiles. This step is fundamental since the magnesium number density acts on the number densities of all the other elements in the state equation. In fact, Ca I and Ca II synthetic profiles obtained now are usually different from those computed with the previous trial model, even though the same Ca abundance is used. If this is the case, we redetermine new values of both Ca abundance and gravity.

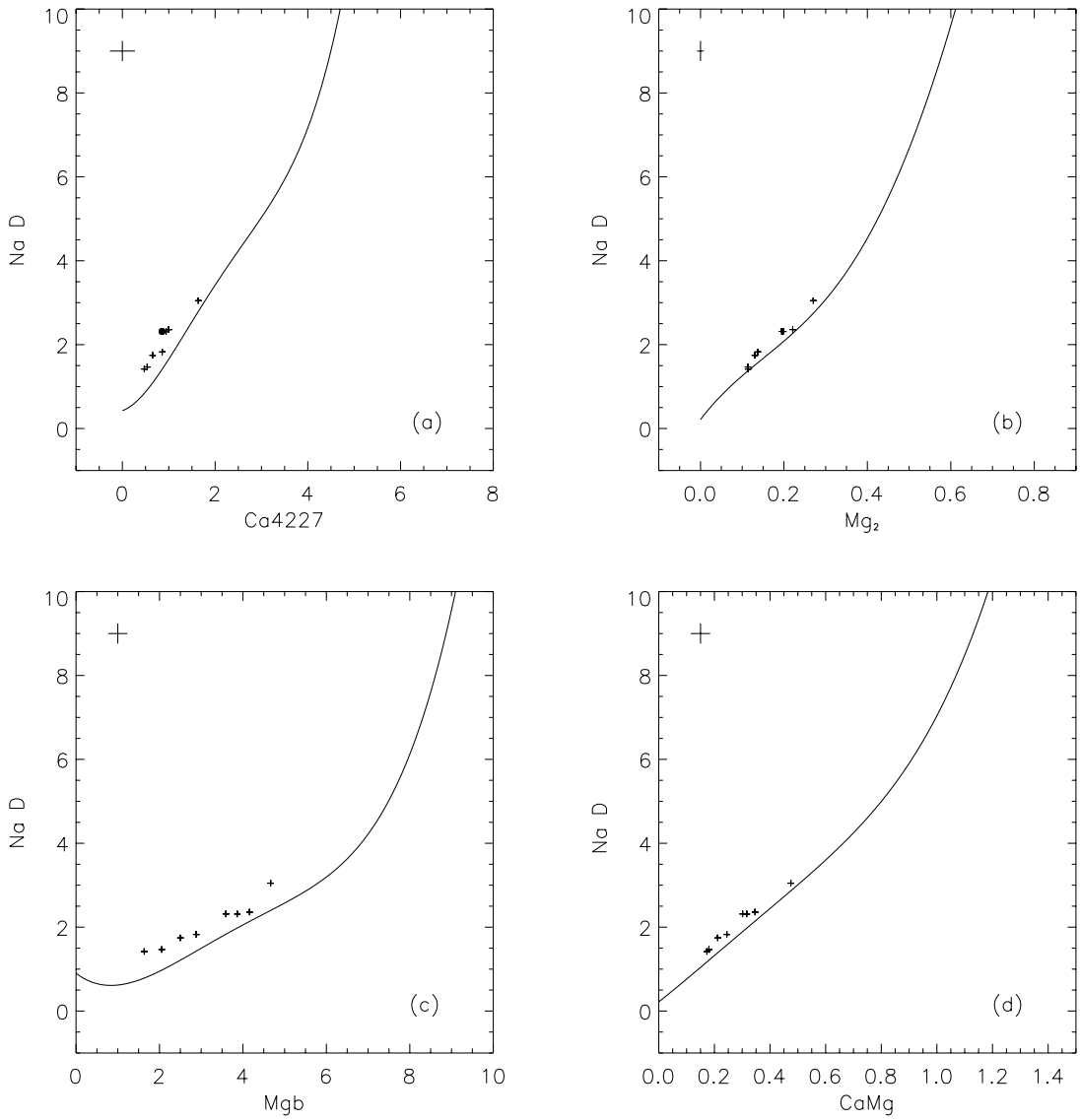


FIG. 13.—Index-index classification diagrams for supersolar stars in B05 (symbols and boundary lines as in Fig. 10).

4. A new ATLAS12 atmosphere model and the corresponding synthetic spectrum are computed with the new Ca, Mg, and Fe abundances, and the procedure is iterated until agreement between observed and computed profiles for Ca II at 8662 Å, Ca I at 6163 Å, Mg I at 5528 Å, and Fe I at 5232 Å is achieved simultaneously.

5. At this point, the whole synthetic spectrum is used to check the ionization equilibrium of Fe I and Fe II. In case of disagreement, we restart the analysis by slightly modifying the $T_{\rm eff}$ of the initial atmosphere model. On the contrary, if the requirement of ionization equilibrium is fulfilled, the $T_{\rm eff}$, log $g$, and the Ca, Mg, and Fe abundances of the atmosphere model are kept fixed, and the synthetic spectrum is used to estimate the abundances of the other elements. In particular, observed and computed spectra are compared in several selected regions, where most of the lines adopted by AP04, Chen et al. (2003), and Tomkin et al. (1997) lie.

6. Finally, a new ATLAS12 model computed with the derived individual elemental abundances is used to generate a new synthetic spectrum that is double-checked. Usually, the agreement with the observed spectrum is so good that no further or only negligible abundance changes are required, leading to the final results. A final consistency check is performed by computing synthetic $(B - V)$ and $(V - I)_{\rm C}$ color indices and by checking the agreement with the observed values.

#### 4.5.3. *Results*

Table 5 shows the starting and final atmosphere model parameters and the derived elemental abundances relative to the solar ones (Grevesse & Sauval 1998). A comparison of the observed and computed spectra covering the Mg I region is shown in Figure 16, while results in more extended regions (four 100 Å wide ranges including Fe I 5232.405 Å, Mg I 5552.405 Å, Ca I 6162.173 Å, Ca II 8662 Å at 6 Å intervals) are available on the Web.[14] The top panel shows the comparison of the observed and computed spectra for HD 125072, while in bottom panel shows, as a reference check of the accuracy of the line data, the same kind of comparison for the Sun (Solar Flux Atlas from Kurucz et al. 1984). The lack of hyperfine structure and/or isotopic shifts in some of the lines in our lists may give rise to

[14] See http://wwwuser.oat.ts.astro.it/castelli/stars.html.

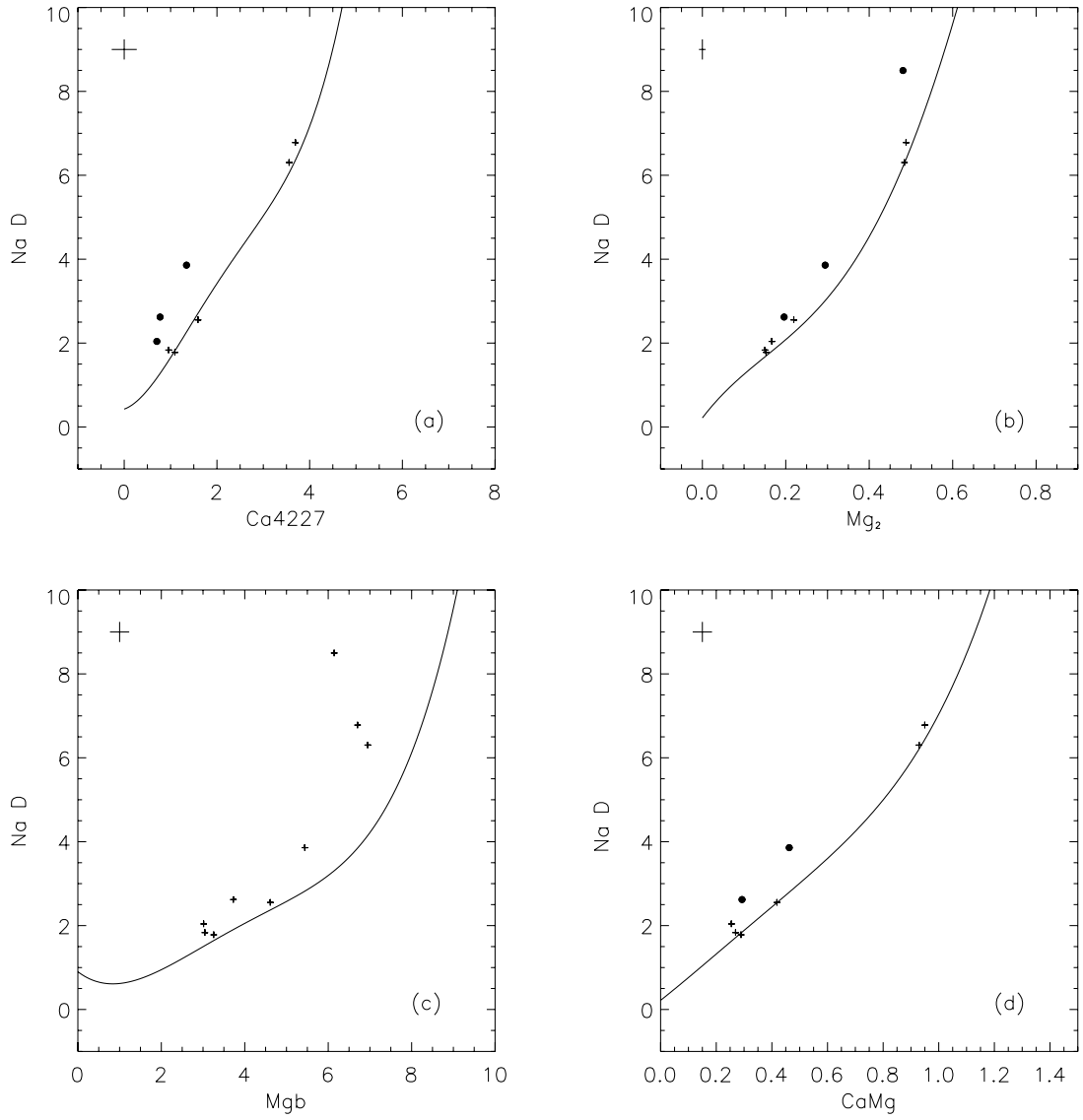


FIG. 14.—Index-index classification diagrams for supersolar stars in LH05 (symbols and boundary lines as in Fig. 10).

pronounced local discrepancies between the synthetic spectrum and the observed one (see also Kurucz 1993). Therefore, we did not use these lines to derive stellar abundances in order to avoid wrong conclusions. This problem is particularly important for such elements like Sc, V, Mn, Co, and Cu.

It is worthwhile to note that we do not find in our analysis any of the quite large systematic difference in the abundances derived from neutral and first ionized Fe and Ca lines found by AP04. Our final model has a higher effective temperature than that of the AP04 model ($T_{\rm eff} = 4950$ K instead of 4671 K), practically the same surface gravity ($\log g = 4.60$ dex instead of 4.62 dex), and is less overabundant [Fe/H] (+0.40 instead of +0.49). The synthetic $(B - V)$ and $(V - I)_{\rm C}$ color indices are 0.99 and 1.02, respectively, and agree within the observational uncertainties with the *Hipparcos* Catalog values [$(B - V) = 1.02 \pm 0.03$ and $(V - I)_{\rm C} = 1.02 \pm 0.02$].

Our main conclusion is that the abundance ratios of $\alpha$-elements, O, Mg, Si, Ca, and Ti over Fe, are +0.0, +0.0, +0.0, −0.07, and +0.00, respectively. The uncertainties on the derived abundances are mostly related to those of the model parameters and atomic data of the lines selected for the analysis. We experimented that an increase or decrease of $T_{\rm eff}$ by 50 K requires a decrease or increase of $\log g$ by 0.1 dex, respectively, in order to obtain synthetic spectra that still reproduce simultaneously the four strong lines of Fe I at 5232 Å, Mg I at 5528 Å, Ca I at 6163 Å, and Ca II at 8662 Å. Although the agreement between the different ionization states may be slightly altered due to the use of different parameter values, the effect on the abundances is negligible ($\pm 0.05$ dex) in general, and the ratio [$\alpha$/Fe], in particular, does not change. On the contrary, very different abundances can be deduced from different lines of the same element, since the uncertainties affecting the atomic and molecular data are large. Furthermore, effects due to inaccurate atomic and molecular data are enhanced in cool metal-rich stars and may give abundance uncertainties on the order of 0.2–0.3 dex or more. Just to minimize such a source of error we performed a differential analysis relative to the Sun and analyzed very large spectral regions. We conclude that the chemical composition of HD 125072 is not $\alpha$-enhanced, thus confirming the findings from our method. In a forthcoming paper F. (Castelli et al. 2005, in preparation), we will apply the same kind of self-consistent high-resolution analysis adopted for HD 125072 to several other spectra in our data sets with the aim of providing homogeneous and reliable elemental abundances of supersolar stars.

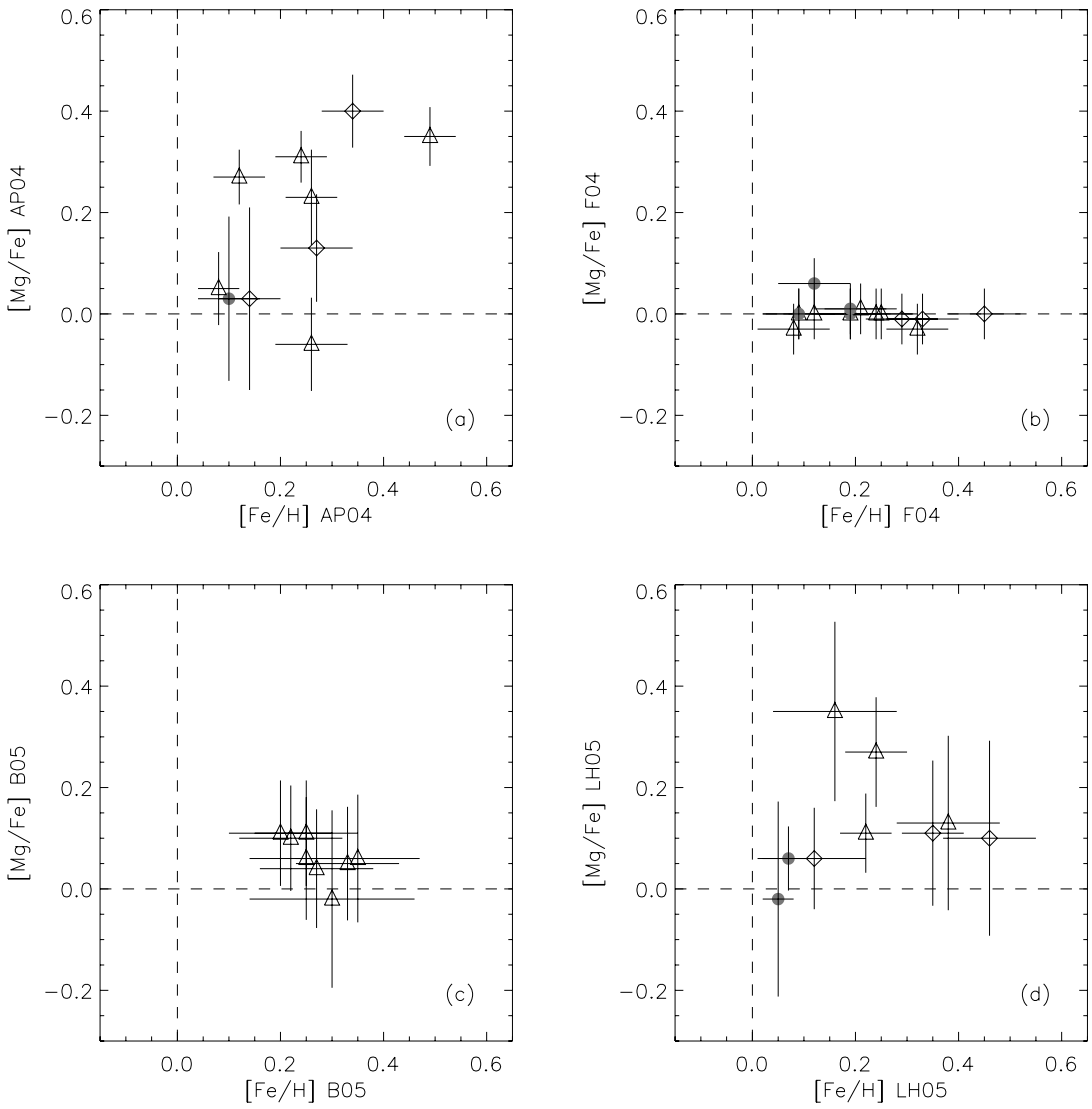


FIG. 15.—Comparison of our classification results with [Mg/Fe] vs. [Fe/H] from (*a*) AP04, (*b*) F04, (*c*) B05, and (*d*) LH05. Possible NSSA, possible SSA, and high-probability SSA stars are indicated by gray filled circles, triangles, and diamonds, respectively.

TABLE 5

[X/H] Elemental Abundances for HD 125072 Relative to the Solar Abundances (Grevesse & Sauval 1998)

| Element | Value |
|---|---|
| C | +0.5 |
| O | +0.4 |
| Na | +0.5 |
| Mg | +0.4 |
| Al | +0.6 |
| Si | +0.4 |
| Ca | +0.33 |
| Sc | +0.2 |
| Ti | +0.4 |
| V | +0.4 |
| Cr | +0.4 |
| Mn | +0.5 |
| Fe | +0.4 |
| Co | +0.4 |
| Ni | +0.5 |
| Cu | +0.4 |
| Zn | +0.3 |
| Y | +0.4 |
| Zr | +0.2: |
| Ba | +0.2 |
| Nd | +0.1 |
| Others | +0.4 |

Notes.—Initial model parameters: $T_{\rm eff} = 4950$ K, $\log g = 4.5$ dex, [M/H] = [+0.5], solar-scaled abundances. Final model parameters: $T_{\rm eff} = 4950$ K, $\log g = 4.6$ dex, individual elemental abundances.

## 5. CONCLUSIONS

More than 100 supersolar stars in the solar neighborhood have been searched for $\alpha$-enhancement via index-index diagrams built with measured or newly computed Lick IDS indices. This method allow us to discriminate NSSA from SSA stars without requiring the previous knowledge of the stellar effective temperature, surface gravity, and metallicity, thus avoiding the problem of misclassification due to possible wrong assumption of the $T_{\rm eff}$, $\log g$, and [Fe/H] values. The method is quite valuable for studying large samples of stars since it is based on low-resolution observations and does not require the large amount of observing time needed to get high-resolution spectra. Its main intrinsic limitations are the low sensitivity for studying stars hotter than the Sun and an increase in the number of uncertain classifications due to the use of general boundary lines instead of precise theoretical points as reference. The main result of the analysis suggests that supersolar thin-disk stars do not have supersolar [$\alpha$/Fe] abundance ratios. In fact, only eight of 119 stars show slight indications of deviation from a solar-scaled chemical composition. The comparison of our sample results with data from the literature strongly points to the conclusion that there is no $\alpha$-enhancement in supersolar thin-disk stars, thus confirming the scenario envisaged by current Galaxy chemical evolutionary models.

The comparison of our classification results with published high-resolution analysis results shows that the latter may be affected by systematic errors due to a lack of accurate atmosphere parameters and/or a lack of self-consistency. On the other hand, we show that a self-consistent high-resolution analysis can derive individual elemental abundances consistent with our classification, as in the case of HD 125072. In a forthcoming paper, we will apply to a sample of representative supersolar stars with

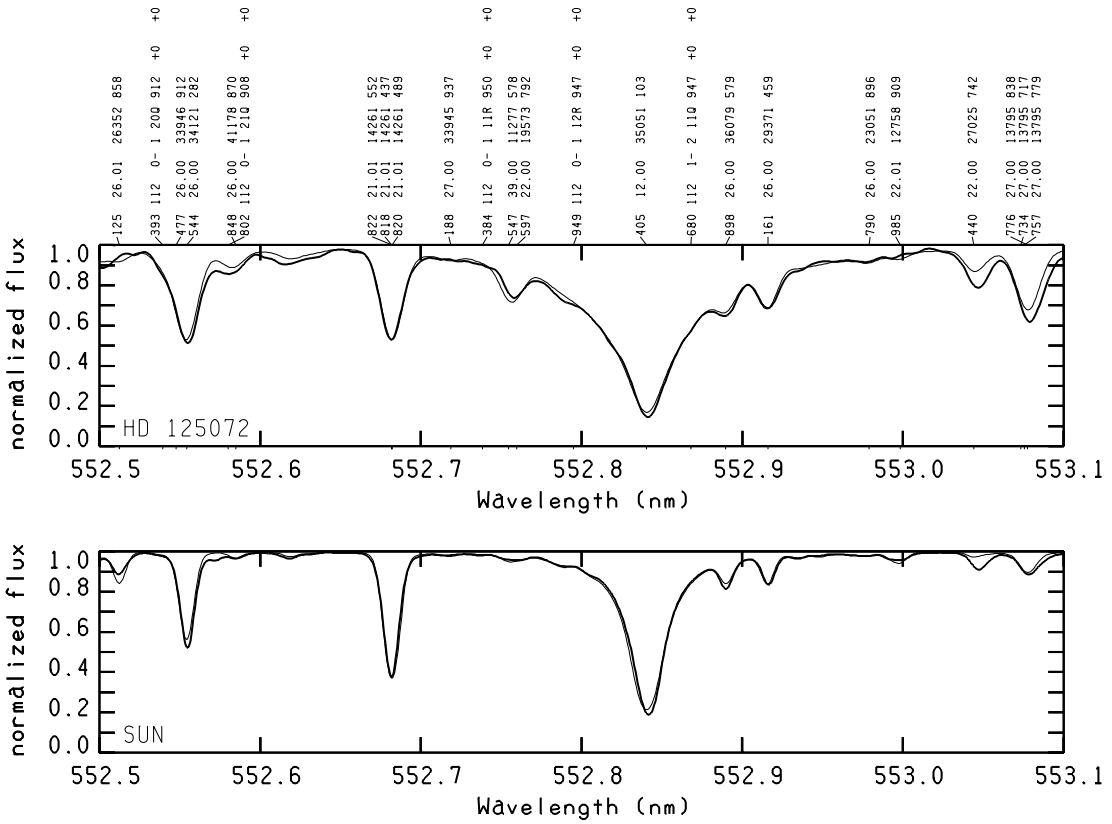


Fig. 16.—Comparison of synthetic spectrum (*thin line*) with observed spectrum (*thick line*) in the Mg I region: HD 125072 (*top*; see Table 5) and the Sun (*bottom*).

contradictory literature estimates of [$\alpha$/Fe] abundance ratios the same kind of self-consistent high-resolution analysis aiming at a sound determination of their detailed chemical composition.

This work received partial financial support from the Mexican CONACyT via grant 36547-E from Università degli Studi di Trieste (60% grants) and from MIUR COFIN-2003028039.

REFERENCES

Allende Prieto, C., Barklem, P. S., Lambert, D. L., & Cunha, K. 2004, A&A, 420, 183 (AP04)
Anstee, S. D., & O'Mara, B. J. 1995, MNRAS, 276, 859
Baade, W. 1958, Ricerche Astron., 5, 3
Barklem, P. S., Piskunov, N., & O'Mara, B. J. 2000, A&AS, 142, 467
Beirão, P., Santos, N. C., Israelian, G., & Mayor, M. 2005, A&A, 438, 251
Bensby, T., Feltzing, S., & Lundström, I. 2003, A&A, 410, 527
Bensby, T., Feltzing, S., Lundström, I., & Ilyin, I. 2005, A&A, 433, 185 (B05)
Bessell, M., Castelli, F., & Plez, B. 1998, A&A, 333, 231
Bonifacio, P., & Caffau, E. 2003, A&A, 399, 1183
Castelli, F. 1999, A&A, 346, 564
Castelli, F., & Kurucz, R. L. 2003, in IAU Symp. 210, Models of Stellar Atmospheres, ed. N. E. Piskunov, W. W. Weiss, & D. Gray (San Francisco ASP), A20
Cayrel, R., Faurobert-Scholl, M., Fautrier, N., Spielfieldel, A., & Thevenin, F. 1996, A&A, 312, 549
Chen, Y. Q., Zhao, G., Nissen, P. E., Bai, G. S., & Qiu, H. M. 2003, ApJ, 591, 925
Chmielewski, Y. 2000, A&A, 353, 666
Franchini, M., Morossi, C., Di Marcantonio, P., Malagnini, M. L., Chavez, M., & Rodríguez, L. 2004a, ApJ, 601, 485 (Paper I)
———. 2004b, ApJ, 613, 312 (Paper II)
———. 2005, in Proc. ESO Astrophys. Symp.,Chemical Abundances and Mixing in Stars in the Milky Way and its Satellites, ed. S. Randich & L. Pasquini (Berlin: Springer), in press (FR05)
Freeman, K., & Bland-Hawthorn, J. 2002, ARA&A, 40, 487
Fuhrmann, K. 2004, Astron. Nachr., 325, 3 (F04)
Gray, R. O., Corbally, C. J., Garrison, R. F., McFadden, M. T., & Robinson, P. E. 2003, AJ, 126, 2048
Grevesse, N., & Sauval, A. J. 1998, Space Sci. Rev., 85, 161
Heiter, U., & Luck, R. E. 2003, AJ, 126, 2015
Kotoneva, E., Flynn, C., Chiappini, C., & Matteucci, F. 2002, MNRAS, 336, 879
Kurucz, R. L. 1993, Phys. Scr., 47, 110
Kurucz, R. L., Furenlid, I., Brault, J., & Testerman, L. 1984, Solar Flux Atlas from 296 to 1300 nm (Sunspot, NM: NSO)
Latham, D. W., Stefanik, R. P., Torres, G., Davis, R. J., Mazeh, T., Carney, B. W., Laird, J. B., & Morse, J. A., AJ, 124, 1144
Le Borgne, J.-F. et al. 2003, A&A, 402, 433
Luck, R. E., & Heiter, U. 2005, AJ, 129, 1063 (LH05)
Malagnini, M. L., Franchini, M., Morossi, C., Di Marcantonio, P. 2005, in Proc. *Gaia* Symp., The Three-dimensional Universe with *Gaia*, ed. C. Turon, K. S. O'Flaherty, & M. A. C. Perryman (ESA SP-576; Noordwijk: ESA), 595
Matteucci, F. 2004, in Proc. Baryons in Dark Matter Halos, ed. R. Dettmar, U. Klein, & P. Salucci (Trieste: SISSA), 72.1
Melendez, J., & Ramirez, I. 2005, in ASP Conf. Ser. 336, Proc. Cosmic Abundances as Records of Stellar Evolution and Nucleosynthesis in honor of Dr. D. Lambert, ed. F. N. Bash & T. G. Barnes (San Francisco: ASP), 343
Mishenina, T. V., Soubiran, C., Kovtyukh, V. V., & Korotin, S. A. 2004, A&A, 418, 551
Morossi, C., Di Marcantonio, P., Franchini, M., Malagnini, M. L., & Chavez, M. 2002, ApJ, 577, 377
Nissen, P. E. 2004, in Origin and Evolution of the Elements, ed. A. McWilliam & M. Rauch (Cambridge: Cambridge Univ. Press), 154
———. 2005, in Proc. *Gaia* Symp., The Three-dimensional Universe with *Gaia*, ed. C. Turon, K. S. O'Flaherty, & M. A. C. Perryman (ESA SP-576; Noordwijk: ESA), 121
Nordström, B., Mayor, M., Andersen, J., Holmberg, J., Pont, F., Jorgensen, B. R., Olsen, E. H., Udry, S., & Mowlavi, N. 2004, A&A, 418, 989
Oort, J. H. 1926, Observatory, 49, 302
Prugniel, Ph., & Soubiran, C. 2004, preprint (astro-ph/0409214)
Reddy, B. E., Tomkin, J., Lambert, D. L., & Allende Prieto, C. 2003, MNRAS, 340, 304
Sbordone, L., Bonifacio, P., Marconi, G., Buonanno, R., & Zaggia, S. 2005, A&A, 437, 905
Spite, M., et al. 2005, A&A, 430, 655
Taylor, B. J. 1999, A&AS, 134, 523
———. 2003, A&A, 398, 731
Tomkin, J., Edvardsson, B., Lambert, D. L., & Gustafsson, B. 1997, A&A, 327, 587
Valdes, F., Gupta, R., Rose, J. A., Singh, H. P., & Bell, D. J. 2004, ApJS, 152, 251
Worthey, G., Faber, S. M., Gonzalez, J. J., & Burstein, D. 1994, ApJS, 94, 687